Fall 2011

Computational studies of ion transport in polymer electrolytes

Hui Wu
Louisiana Tech University

COMPUTATIONAL STUDIES OF ION TRANSPORT IN

POLYMER ELECTROLYTES

by

Hui Wu, B.S., M.S.

A Dissertation Presented in Partial Fulfillment
of the Requirements for the Degree
Doctor of Philosophy

COLLEGE OF ENGINEERING AND SCIENCE
LOUISIANA TECH UNIVERSITY

November 2011

UMI Number: 3492480

LOUISIANA TECH UNIVERSITY

THE GRADUATE SCHOOL

November, 2011
_____
Date

We   hereby   recommend   that   the   dissertation   prepared   under   our   supervision

by Hui Wu
_____

entitled _____

Computational Studies of Ion Transport in Polymer Electrolytes
_____

_____

_____

_____

be   accepted   in   partial   fulfillment   of   the   requirements   for   the   Degree   of

Ph.D in Engineering
_____

_____
Supervisor of Dissertation Research

_____
Head of Department

Physics
_____
Department

Recommendation concurred in:

_____

_____

_____   Advisory Committee

_____

Approved:

_____
Director of Graduate Studies

_____
Dean of the College

Approved:

_____
Dean of the Graduate School

ABSTRACT

Improving ionic conductivity and lithium mobility in polymer electrolytes is important for their practical use for battery electrolytes. In this study, a combination of molecular dynamics and Monte Carlo simulations was used to bring insight into lithium ion transport in poly(ethylene oxide) (PEO) with plasticizers and also next to alumina solid surface doped with lithium salt. The simulations were performed using a moderately high molecular weight polymer (M_n = 10,000 g/mol) at an EO:Li ratio of 15. For the plasticized system, the PEO with $LiN(CF_3SO_2)_2$ (LiTFSI) was mixed with 10 wt% plasticizers that included either cyclic ethylene carbonate (EC) or propylene carbonate (PC). Comparisons with an array of experiments showed a slight underestimation of the compared ionic conductivity, but within a factor of two, at most. With the addition of EC and PC plasticizers, the ionic conductivity increased a moderate degree with most of the increase due to faster TFSI anion motion, but not lithium cation. It was found that propylene carbonate formed complexes with the TFSI anion, in which lithium was an intermediary, creating moderate sized clusters. This formation allowed enhanced diffusion of lithium ions bound with TFSI ions, but this formation was offset by slower diffusion for lithium ions bound with ethylene oxide oxygens. Ethylene carbonate, on the other hand, showed no significant complexing with TFSI anion. The formation of this cluster, therefore, may be an avenue for increasing lithium diffusion but would likely require a plasticizer with stronger interactions with lithium than the carbonates studied.

We also examined the influence of both acidic and basic alumina surfaces on the structure and lithium mobility in PEO with $LiClO_4$ salts. The results showed the surface interacted with lithium salt anion in the acidic case via hydrogen bonding, which essentially freezes the lithium salt anion movement at the surface, yet a modest enhancement in lithium ion mobility was observed at low temperature.

APPROVAL FOR SCHOLARLY DISSEMINATION

The author grants to the Prescott Memorial Library of Louisiana Tech University the right to reproduce, by appropriate methods, upon request, any or all portions of this Dissertation. It is understood that "proper request" consists of the agreement, on the part of the requesting party, that said reproduction is for his personal use and that subsequent reproduction will not occur without written approval of the author of this Dissertation. Further, any portions of the Dissertation used in books, papers, and other works must be appropriately referenced to this Dissertation.

Finally, the author of this Dissertation reserves the right to publish freely, in the literature, at any time, any or all portions of this Dissertation.

Author _____

Date _____

TABLE OF CONTENTS

LIST OF TABLES

LIST OF FIGURES

ACKNOWLEDGMENTS

I would like to thank Dr. Collin Wick for his guidance, support and encouragement during my graduate career, and for providing me chances to experience so many memorable moments and understand scientific research deeply. His great knowledge of thermodynamics and statistical mechanics constantly aided in solving many of the scientific problems which I crossed. I would like to thank also Dr. Weizhong Dai, Dr. Pedro Derosa, Dr. Sven Eklund and Dr. Bala Ramachandran for taking time to serve on my committee. I would like to thank Jeramia Kurt Evans for his great help and friendship. I, furthermore, thank all group members and my friends for their advice, assistance and valuable friendship. Finally, the constant support from my husband, Shenghua Ni, and the joy from my son David Ni, has helped me keep going when things got tough. I could not have even gotten near the point where I am now without my parents, Weili Wu and Yuying Li, and my sister (Suxiang Wu) and her husband (Gongbin Gu), for their endless love and support and encouragement throughout my entire life.

CHAPTER 1

INTRODUCTION AND MOTIVATION

This work focuses on using computational techniques to comprehend why plasticized and nanocomposite solid polymer electrolyte (SPE) membranes have enhanced conductivity with respect to pure SPEs. The long-term goal of this work is to provide guidance to engineer new polymeric materials to replace traditional liquid electrolytes for rechargeable lithium batteries (RLBs). This replacement can only be done if a reliable molecular picture can be developed, which requires verification. This verification is a major factor of the work in which numerous comparisons with experiment have been carried out, the most important of which are comparisons with ionic conductivities.

The need for energy is one of the most important issues and challenges facing our country and the world today. Improving electrochemical energy technologies, for example, batteries will be a vital part of the solution to our energy challenges. Economic and environmental benefits will be provided through these new technologies. Their use can also directly reduce the dependence on imported fuels. In recent decades, rechargeable lithium batteries, especially the second generation, have been used increasingly in consumer electronics and military equipment, and have the potential for utilization in electric and hybrid vehicles [1-6].

The most often used electrolytes for RLBs are liquids. However, the leakage of liquid electrolytes is a major safety concern due to the highly reactive elements such as lithium salts and metals. Furthermore, at high temperatures and in overcharging circumstances, traditional carbonate electrolytes react with the electrodes, creating gases that cause the batteries to break, resulting in fire or explosion [7-11]. Due to the electrolyte reaction, some of the lithium becomes passivated and isolated from the bulk anode as finely divided lithium. This phenomenon is common for second generation lithium cells and is somewhat independent of the cathode [7].

To eliminate these problems, a solid polymer electrolyte (SPE) can be used in place of the liquid electrolytes since it is virtually free of leakage. These composite solid polymer electrolytes offer other potential advantages, such as low cost design, flexibility in sizes and shapes, good electrochemical stability, enhanced mechanical properties, low flammability, low corrosive properties, reduce propensity for leakage, and the ability to form good interfacial contact with electrodes [5, 12, 13]. The most investigated SPE is poly(ethylene oxide) (PEO) with the addition of lithium salts of the imide anion, $LiClO_4$ [14-29], $Li[N(CF_3SO_3)_2]$ (LiTFSI) [30-32] , $LiCF_3SO_3$ (LiTf) [14, 33-39], LiI [14, 40, 41], and $LiBF_4$ [42], to allow the conduction of lithium ions, in which the segmental motion of the PEO chains assist in ion motion along the oxygen atoms. The ionic conductivity of SPEs at room temperature is on the order of $10^{-4} \sim 10^{-7}$ S/cm due to its high crystalline ratio [13], while 10^{-3} S/cm is a good fit for an electrolyte to be commercially viable [5, 6, 43, 44]. A reasonable speculation for this non-viability is that the nature of SPEs are crystalline near room temperature, hindering their efficiency and significantly reducing their practicality [45]. Thus, diverse studies of trying to minimize the crystallization

degree on the polymer electrolyte and modifying the composites have been pursued to improve ionic conductivity of polymer electrolytes since the middle of the 1980s [12]. Two of the most popular methods [46] pursued to improve the conductance of SPEs are the introduction of plasticizers [6, 45, 47-50], often creating polymeric gels, and the utilization of nanoporous membranes,[2, 19, 51] which keep the solid-state character of the PEs intact.

1.1   Plasticized Polymer Electrolytes

The addition of plasticizers, such as cyclic carbonates like propylene carbonate (PC) and ethylene carbonate (EC) [20, 22, 38-41], has been shown to increase the conductivity close to practical levels around 10^{-4} S/cm at room temperature [14, 46, 52-56]. Consider the beneficial properties of SPEs and the high conductivities of liquid electrolytes, plasticized polymers have both properties. While plasticized polymer electrolytes provide conductivities close to those of liquid electrolytes, they have two main weaknesses. Since a large liquid component is added to the polymer, the mechanical properties are weakened with respect to SPEs. Furthermore, the separation of the liquid fraction from the polymer, indicated as syneresis, can be a problem and lead to electrolyte breakdown [57]. There are multiple ways to improve the mechanical properties of gel polymer electrolytes, including cross-linking the polymers,[58] and placing low molecular weight polymer, e.g. PEG (M_w= 200~6000) [17, 20, 26, 29, 36, 59, 60] into a network of cross-linked fumed silica [61].

1.2 Nanocomposite Polymer Electrolytes

In order to reduce the crystallization degree on the polymer electrolyte without affecting the mechanical properties of the system, inorganic and/or organic additives are added to the SPEs, which are generally called "composite solid polymer electrolytes" (CSPEs). Various materials, such as ceramic powders [24], organic acids [60], and organic/inorganic composites [62], have been examined for the purpose of producing CSPEs. These organic/inorganic materials include, γ-LiAlO$_2$ [15, 21, 22, 41, 63-66], and Al$_2$O$_3$ [2, 15, 17, 21, 22, 24-27, 35, 40, 41, 63, 67-70], SiO$_2$ [15, 23, 28, 37, 42, 60, 63, 67, 71], TiO$_2$ [2, 22, 23, 63, 67, 68, 70], Fe$_2$O$_3$ [63], SrBi$_4$Ti$_4$O$_{15}$ (SBT (CIT)) [22], MgO [41], and other filler compounds. Unlike plasticized SPEs, CSPEs have very good mechanical properties and improved conductivities over pure SPEs. They also are not prone to leakage, but still have conductivities that are around two orders of magnitude too low for practical use. With the introduction of spherical nanoparticles, an increase in the amorphous regions of the polymer has been linked to higher conductivity [2, 72]. Experiment often reveals that stronger PEO oxygen-nanoparticle and anion-nanoparticle interactions aid faster lithium transport through the electrolyte [17, 26, 73]. However, for short chained PEO, evidence shows that the crystallinity can facilitate lithium ion transport, thereby making crystallinity a possible ion transport enhancer [74]. Due to the interactions between lithium, its counter ion, and the nanoparticles, higher conductivity and lithium transference are achieved within the composite membranes [73]. A desirable outcome from this interaction is a faster lithium diffusion rate with respect to anion diffusion. This faster rate is important because only the lithium undergoes oxidation and reduction at the electrode surfaces.

Another pathway is to introduce nanoporous membranes (e.g. TiO_2, Al_2O_3, and SiO_2 etc.) to SPEs, which has the possible benefit of increasing the solid-polymer interfacial area over the spherical nanoparticles [75-80]. Evidence has shown that the stronger the PEO oxy-nanoparticle/anion-nanoparticle interactions, the faster lithium transport facilitation throughout the electrolytes [17, 26, 73]. The previous statement implies that increasing both the interaction strength and volume fraction of PEO in connection with these interactions may increase the overall conductivity and transference of lithium. Recent research shows that the ionic conductivity and microstructure of composite SPEs from the Lewis acid-base type interactions varied between acidic and basic type species present in the systems studied [16, 26, 68, 73, 81]. The Lewis acid groups of the surface (e.g. the -OH group on the Al_2O_3 surface) may result in a higher conductivity than that of the corresponding Lewis base sample. Based on this reasoning, further strengthening of these interactions and increasing the overall volume fraction of PEO in touch with these interactions will enhance the conductivity and lithium transference number.

1.3   Computational Methods Needed

The understanding of the ion transport mechanism on the molecular level of these systems and the effects of these behaviors on the entire conductivities of SPEs would benefit the design of SPEs for RLBs greatly. Experimental methods can bring some insight into the effect of plasticizers on polymer structures. However, computational methods play a valuable role in providing significant insight into molecular level interactions and structures. Particularly, molecular dynamics (MD) simulations are well suited for providing a direct route from the microscopic details of a system (the molecular

geometry, the masses of the atoms, the interaction between them, etc.). The results of macroscopic properties, such as ionic conductivity, transport coefficients, and so on may also be directly compared with those of real experiments.

The conduction mechanism of lithium in PEO and carbonates has been investigated widely with the use of computational methods [82-96]. Because of this extensive investigation, there is a good understanding of the mechanism of lithium ion transport in neat amorphous and crystalline PEO. Nevertheless, the role of plasticizers on lithium conduction in PEO in low enough concentrations to be relevant for RLBs has not been studied computationally. This study requires the development of new computational methodologies.

Since computational methods can provide a direct picture of the molecular structure, a deeper understanding of the system details can be obtained. For example, the system details may illustrate how the conductivities of SPEs would be beneficial for SPE and RLB design. Different experimental methods may elucidate the effects of nanoparticles on polymer structures such as neutron scattering [97], Raman spectroscopy [98], and NMR [76, 99], but computational methods provide a much more distinct molecular level picture than these methods.

Regarding the modeling of SPEs with nanoparticles, there have been a few studies focused on lithium ion transport on the molecular level [100, 101]. These works provide some interesting qualitative insight into lithium ion motion for these systems. Computational methods have been used extensively to study conduction mechanisms [83, 92, 102] such as that for the lithium in PEO. These methods have revealed an in-depth understanding of the conduction mechanism for lithium ion transport in both amorphous

and crystalline PEO. Other studies of nanoparticle embedded polymer electrolytes have been carried out, but without adequate comparisons with experiments [100, 101].

The effect of nanoparticles on the mechanism of lithium conduction at the molecular level is not understood completely. Research of interactions between PEO, lithium, and its counter-ions with spherical nanoparticles affecting the lithium ion conduction is still incomplete and lacks in comparison with other experiments. Sometimes, molecular simulation is questionable even though it is an exceptional method for understanding the details of molecular levels. Experimental comparisons with nanocomposite systems can be complex because the long range orders are not tracked by the usual molecular simulation methods. A new strategy is needed to allow for a more direct comparison between these different molecular systems, in turn, providing an improvement in molecular simulation. When used in conjunction with an experiment, the factors may be better understood in order to maximize the nanocomposite conductivity lithium transference.

CHAPTER 2

COMPUTER SIMULATION TECHNIQUES

2.1 Statistical Mechanics

2.1.1 Sampling from Ensembles

Statistical mechanics provides a link for relating the microscopic properties (e.g atomic and molecular positions **R**, velocities v) of atoms and molecules to the macroscopic properties (e.g. pressure p, internal energy E) of materials. Consider a one-component macroscopic system, which is usually defined by a small set of parameters (e.g. the number of particles N, the temperature T, the energy E, the volume V and the pressure p). We use Γ for a point in phase space and calculating the instantaneous value of some macroscopic property A, as a function $A(\Gamma)$. The experimentally observable 'macroscopic' property A_{obs} can be calculated by averaging over all possible states $A(\Gamma)$:

$$A_{obs} = \langle A \rangle_{ensemble} = \sum_{\Gamma} A(\Gamma)\rho_{ensemble}(\Gamma), \qquad \text{Eq. 2.1}$$

where $\rho(\Gamma)$ is the probability density for state Γ. In general, $\rho_{ensemble}$ such as ρ_{NpT} and ρ_{NVT}, and, is a function defined by the chosen fixed macroscopic parameters. For convenience, $\rho_{ensemble}(\Gamma)$ can be written as a 'weight' function $w_{ensemble}(\Gamma)$, with a partition function $Q_{ensemble}$ (also called the sum over states) acting as the normalizing factor:

$$P_{ensemble}(\mathbf{\Gamma}) = \frac{w_{ensemble}(\mathbf{\Gamma})}{Q_{ensemble}}$$

Eq. 2.2

$$Q_{ensemble} = \sum_{\mathbf{\Gamma}} w_{ensemble}(\mathbf{\Gamma})$$

Eq. 2.3

$$\langle A \rangle_{ensemble} = \frac{\sum_{\mathbf{\Gamma}} A(\mathbf{\Gamma}) w_{ensemble}(\mathbf{\Gamma})}{\sum_{\mathbf{\Gamma}} w_{ensemble}(\mathbf{\Gamma})} .$$

Eq. 2.4

2.1.2 Common Statistical Ensembles

The four most popular ensembles are the following: the micro-canonical (constant-NVE) ensemble, the canonical (constant-NVT) ensemble, the isothermal-isobaric (constant-NpT) ensemble, and the grand canonical (constant-μVT) ensemble [103, 104]. In this work, the first three ensembles are used and explained below.

Microcanonical Ensemble Q_{NVE}. The microcanonical ensemble, also referred to as the constant-NVE ensemble, is very useful for theoretical discussions. This ensemble is a theoretical tool used to represent the thermodynamic properties of an isolated system. In such a system, all macrostates have the same number of particles (N), volume (V), and energy (E). Figure 2.1 describes a completely isolated system, as it does not exchange energy or mass with the rest of the universe.
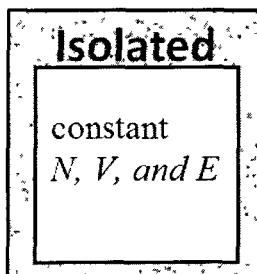
Figure 2.1 Illustration of microcanonical ensemble. Isolated system is suspended in an insulating wall

The probability density for the microcanonical ensemble yields $\delta(H(\Gamma)\text{-}E)$, where H is the Hamiltionian of the system and δ is the Kronecker delta, which is zero if the set of states are discrete or one if the states are continuous. Then the micro-canonical partition function can be written:

$$Q_{NVE} = \sum_{\Gamma} \delta(H(\Gamma) - E).$$

Eq. 2.5

For a quasi-classical system, the partition function can be expressed using a factor of $1/N!$,

$$Q_{NVE} = \frac{1}{N!} \frac{1}{h^{3N}} \int\int \delta(H(\mathbf{r,p}) - E)d\mathbf{r}d\mathbf{p},$$

Eq. 2.6

where h is Planck's constant, $\int\int d\mathbf{r}d\mathbf{p}$ stands for double integrations over all $6N$ phase space coordinates signs on the integral for the $6N$ positions and momenta for the three-dimensional system of N spherical particles.

Canonical Ensemble Q_{NVT}. The most commonly used ensemble in statistical thermodynamics is the canonical, or constant-NVT, ensemble. Each of the systems can exchange energy with a large heat reservoir or heat bath, and each also requires keeping the number of particles (N), the volume (V), constant, and the ensemble has a well-defined temperature (T) (Figure 2.2).
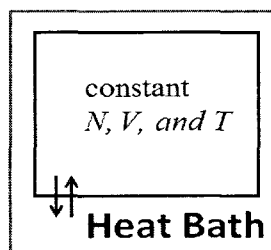
Figure 2.2 Illustration of canonical ensemble. The system of interest is an enclosed system in a bath

For the constant-NVT ensemble, the probability density is corresponding to exp(-$H(\mathbf{\Gamma})/k_BT$) and the partition function yields:

$$Q_{NVT} = \sum_{\mathbf{\Gamma}} \exp(-H(\mathbf{\Gamma})/k_BT).$$

<div align="right">Eq. 2.7</div>

For a canonical ensemble of the total energy, the Hamiltonian H. The Hamiltonian is the sum of kinetic K and potential U energies of a system, $H(\mathbf{\Gamma}) = K(\mathbf{\Gamma}) + U(\mathbf{\Gamma})$, which is assumed that the particles do not have any internal energy I, if so, it would be added to the sum, and treated separately. The usual classical and semiclassical formulations of atoms do not have internal energy terms, but molecules have rotational and vibrational degrees of freedom.

The quasi-classical form for an atomic system is:

$$Q_{NVT} = \frac{1}{N!}\frac{1}{h^{3N}} \int\int \exp(-H(\mathbf{r},\mathbf{p})/k_BT)d\mathbf{r}d\mathbf{p}.$$

<div align="right">Eq. 2.8</div>

Since the kinetic energy K is $\mathbf{p}$-dependent and potential energy U is $\mathbf{r}$-dependent, the energy functions have the set of coordinates $\mathbf{r}_i$ and momenta $\mathbf{p}_i$ for each molecule, the Hamiltonian becomes $H(\mathbf{r},\mathbf{p}) = K(\mathbf{p}) + U(\mathbf{r})$. The partition function can be rewritten as the equation shown below, which is a product of kinetic (ideal gas) and potential (excess) part:

$$Q_{NVT} = \frac{1}{N!}\frac{1}{h^{3N}} \int \exp(-K(\mathbf{p})/k_BT)d\mathbf{p} \int \exp(-U(\mathbf{r})/k_BT)d\mathbf{r}$$
$$= Q_{NVT}^{id}Q_{NVT}^{ex}.$$

<div align="right">Eq. 2.9</div>

The quasi-classical form for an atomic system is:

$$Q_{NVT}^{id} = \frac{V^N}{N!\Lambda^{3N}},$$

<div align="right">Eq. 2.10</div>

where Λ is the thermal de Broglie wavelength and equals to $\sqrt{h^2/2\pi mk_BT}$.

$$Q_{NVT}^{ex} = \frac{1}{V^N} \int \exp(-U(\mathbf{r})/k_B T) d\mathbf{r}.$$ Eq. 2.11

Instead of Q_{NVT}^{ex}, we often use the configuration integral

$$Z_{NVT} = \int \exp(-U(\mathbf{r})/k_B T) d\mathbf{r},$$ Eq. 2.12

where, k_B is Boltzmann constant. The partition function turns to

$$Q_{NVT} = \frac{1}{N! \Lambda^{3N}} \int \exp(-U(\mathbf{r})/k_B T) d\mathbf{r}.$$ Eq. 2.13

As a consequence of the separation of Q_{NVT}, all the thermodynamic properties derived from A can be expressed as a sum of ideal gas and configurational parts. In statistical mechanics, it is easy to evaluate ideal gas properties [105], and we may expect most attention to focus on the configurational functions.

Isothermal-isobaric Ensemble Q_{NpT}. The isothermal-isobaric ensemble (constant-NpT ensemble) is an ensemble of systems in which the individual systems have N, p, and T fixed. The constraints are the total energy and total volume of the ensemble (Figure 2.3).
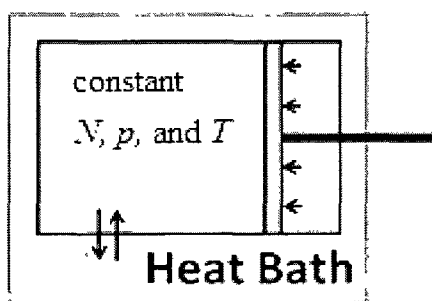
Figure 2.3 Illustration of canonical ensemble. An enclosed system in a bath and a piston is at constant pressure

The density for the NpT ensemble is turned into $\exp[-(H+PV)/k_B T]$ and the partition function is

$$Q_{NpT} = \sum_{\Gamma}\sum_{V} \exp(-(H+PV)/k_B T) = \sum_{V} \exp(-PV/k_B T) Q_{NVT} \ . \qquad \text{Eq. 2.14}$$

The quasi-classical form for an atomic system is:

$$Q_{NpT} = \frac{1}{N!}\frac{1}{h^{3N}}\frac{1}{V_0} \int\int \exp[-(H+PV)/k_B T]dVd\mathbf{r}d\mathbf{p} \ , \qquad \text{Eq. 2.15}$$

where V_0 is a basic unit of volume.

For the isothermal-isobaric ensemble, the configuration integral is

$$Z_{NpT} = \int \exp(-PV/k_B T)dV \int \exp(-U(\mathbf{r})/k_B T)d\mathbf{r} \ . \qquad \text{Eq. 2.16}$$

The constant-NpT ensemble is the most useful, as most experimentalists fix the temperature and pressure when making measurements.

2.2   General Simulation Methods

There are two predominant types of simulation methods that are employed to study and calculate the thermodynamic properties of molecular systems: molecular dynamics (MD) and Monte Carlo (MC).

2.2.1   Monte Carlo (MC) Methods

MC methods include a vast array of methodologies that can be used to tackle many problems. Generally, they are based on using random numbers to integrate a value or sample a system. The most common MC method used for molecular simulation is based on importance sampling, or preferentially sampling "important" regions of phase space. Consider an N particle system, there are $3N$ degrees of freedom, and calculating a property as shown in Eq. 2.4 requires integrating a probability distribution with this many dimensions. In any straightforward numerical integration, the number of points to be integrated will scale exponentially with the number of particles, most of which will be in

configurations with very high energy for any moderately dense systems (i.e. with particle overlaps). However, importance sampling specifically targets regions of phase space that have energies low enough to contribute to the calculation of a property.

Most MC methods that rely on importance sampling create stochastic trajectories, which follow a Markov Chain process. For a Markov Chain, any change in the system configuration of a single step only depends on the previous step itself. In MC, the system moves between different states, from state α to state β, stochastically. A Monte Carlo trajectory is generated by performing a random walk through configuration space with a certain acceptance probability for each step. This acceptance probability, $P_{acc}(\alpha \rightarrow \beta)$, is used to satisfy the condition of "microscopic reversibility", and the asymmetric Metropolis acceptance probability is given by [106]:

$$P_{acc}(\alpha \rightarrow \beta) = \min\left[1, \frac{\rho(\beta)}{\rho(\alpha)} \frac{T(\beta \rightarrow \alpha)}{T(\alpha \rightarrow \beta)}\right],$$ Eq. 2.17

where $\rho(\alpha)$ is the probability density to be in state α, $T(\alpha \rightarrow \beta)$ is the transition probability from state α to state β.

Metropolis Monte Carlo. In the Metropolis method, any transition probability is completely random, and is designed to be symmetric (i.e. there is equal probabilities in going forward and reverse), so the ratio of T is 1. The acceptance probability is given by:

$$P_{acc}(\alpha \rightarrow \beta) = \min\left[1, \frac{\rho(\beta)}{\rho(\alpha)}\right].$$ Eq. 2.18

For molecular systems, the Metropolis MC method is often used to translate particles a random distance and direction, rotate them a random direction and angle, or carry out volume fluctuations (in the NpT ensemble) of random degrees.

Gibbs Ensemble Monte Carlo (GEMC). The Gibbs Ensemble Monte Carlo (GEMC) technique [107-109] is a method used in the equilibrium phase for the simulation. GEMC works on two simulation boxes with an explicit interface kept in either the NVT or NpT ensemble, but in thermodynamic contact (Figure 2.4) [110]. The whole system is kept in either the NVT or NpT ensemble. For the former, the total volume is fixed, while in the latter, the total pressure of the system is fixed. GEMC uses three types of moves: (a) independent particle moves in each box using normal Metropolis method, (b) particle exchanges (or creation/destruction-moves) to equilibrate chemical potentials between phases, and (c) volume moves, either with each other or with an outside pressure bath.
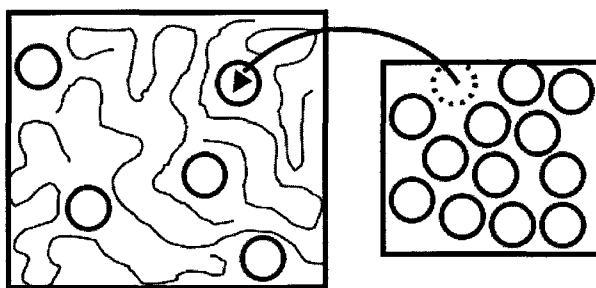
Figure 2.4 Schematic of GEMC technique for polymer and plasticizer (circles), showing a particle exchange move

Connectivity-altering Monte Carlo (CAMC). For the simulation of SPEs, fairly high molecular weight polymers are used. It is known that the simulation of polymers scales geometrically with chain lengths with conventional simulation techniques [111]. The CAMC technique can overcome the limitations born by slow relaxation dynamics [112]. CAMC allows the rearrangement of polymer connectivity of one or more polymers, circumventing polymer chain length as a hindrance to equilibration (Figure 2.5) [113]. This technique relies on the fact that most polymers are polydispersed or that there is a

distribution of polymer chain lengths in a melt. For these simulations, the semi-grand canonical ensemble is utilized, which fixes the total number of particles and the total polymer molecular weight. By reconnecting one polymer chain with parts of another, the configuration of a single polymer can rapidly change, making polymer molecular weight no longer a factor in the ability to equilibrate a molecular system.
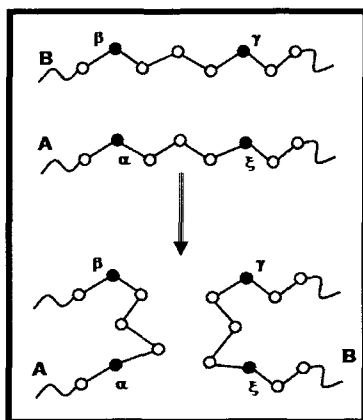
Figure 2.5 Schematic of how a CAMC move works, by reconnecting parts of polymer A with polymer B

2.2.2 Molecular Dynamics (MD)

Molecular Dynamics (MD) is a very useful method of computer simulation of atomic and molecular modeling based on statistical mechanics. In contrast to MC, MD simulations follow deterministic trajectories. MD simulations consist of the numerical, step-by-step, solution of the classical equations of motion. The forces exerting on the atoms may be defined by integrating Newton's second law or the equation of motion: $F_i = m_i \ddot{r}_i$, where the force F_i acting on a particle i of mass m_i in the system and $\ddot{r} = d^2r_i/dt^2$ is its acceleration. The result is a trajectory that describes the positions, velocities and accelerations of the particles in the system as they vary with time [104, 114].

By Verlet in 1967 [115], the first and the most widely used numerical integration scheme, is derived by truncating the Taylor expansion of $\mathbf{r}_i(t+\delta t)$ at $\mathbf{r}_i(t)$,

$$\mathbf{r}_i(t + \delta t) = 2\mathbf{r}_i(t) - \mathbf{r}_i(t - \delta t) + \ddot{\mathbf{r}}_i(t)\delta t^2 + \mathcal{O}(\delta t^4),\qquad \text{Eq. 2.19}$$

$$\mathbf{v}_i(t) = \frac{\mathbf{r}_i(t + \delta t) - \mathbf{r}_i(t - \delta t)}{2\delta t} + \mathcal{O}(\delta t^2).\qquad \text{Eq. 2.20}$$

The MD method is deterministic, the state of the system can be predicted at any time in the past or future by the positions and velocities of each atom. To minimize numerical errors, a very small simulation timestep is chosen often near 1 fs $= 10^{-15}$ s. This timestep can be a disadvantage as a typical MD simulation trajectory generally is no longer than a few nanoseconds, with rare simulations of a microsecond carried out, which require very large amounts of computer power and time. However, the basic MD method is quite standard and can be used to study a large variety of systems, allowing for its wide use by experts and novices alike.

2.3 Computer Experiments

MC and MD simulations are used individually or in concert to carry out the investigation of molecular systems, and to calculate and bring molecular level insight into dynamics and structural properties. Below are the common methods for the calculation of these properties, and other special methods used in this work are described in related chapters.

2.3.1 Conductivity (λ)

One of the most important aspects in evaluating the quality of SPEs is determining their conductivity. Maximizing ionic conductivity is important for battery operation as higher conductivity is linked to greater current. To calculate the conductivity

(λ) of the system, the Einstein relation was used by double summing over all ionic species (N) [84, 85, 116],

$$\lambda = \lim_{t\to\infty} \frac{e^2}{2dtVk_BT} \sum_{i=1}^{N}\sum_{j=1}^{N} z_i z_j \left\langle [\mathbf{r}_i(t) - \mathbf{r}_i(0)] \bullet [\mathbf{r}_j(t) - \mathbf{r}_j(0)] \right\rangle, \qquad \text{Eq. 2.21}$$

where e presents the electron charge, V is the volume of simulation box, k_B is Boltzmann constant; T is the thermodynamic temperature in Kelvin; t is the time; d is the dimension of the movement ($d = 3$ for three dimensions) N is the total number of cations and anions in the simulation system; $\mathbf{r}_i(t)$ represents the position vector of ith ion with respect to time; z_i and z_j are the charge over ions i and j. $\langle\ \rangle$ indicates the ensemble average.

2.3.2 Transport Coefficient (D) and Transference Number (τ_+)

Another tract of understanding is that interaction of lithium and its counterion with added species are responsible for both higher conductivity and lithium transference in the composite membranes. High lithium transference points to a faster lithium diffusion rate with respect to anion diffusion, and this faster diffusion rate is desirable since only lithium is oxidized and reduced at electrodes. Diffusion is caused by the spread of particles through random motion in a nonhomogeneous fluid from regions of higher to lower concentration. The self-diffusion (D) is defined as the diffusion coefficient of the species when the chemical potential gradient is zero. It can be evaluated for each ionic species in two ways. One is fairly straightforward in MD simulations using the Einstein relation [104, 114, 116]:

$$D_i = \lim_{t\to\infty} \frac{\langle MSD(t)\rangle}{2dt} = \lim_{t\to\infty} \frac{\left\langle [\mathbf{r}_i(t) - \mathbf{r}_i(0)]^2 \right\rangle}{2dt}, \qquad \text{Eq. 2.22}$$

where the mean square displacement $MSD(t)$ is a measure of the average distance a given particle, or molecule's center-of-mass in a system travels at time t; $\langle\ \rangle$ represents the

ensemble average,$r_i(t)$ represents the vector position of species i at time t, d is the dimension of the movement.

The other way to obtain diffusion coefficient (D) is from the velocity autocorrelation function for a long time (τ) period by using Green –Kubo relation.[114]:

$$D_i = \frac{1}{d} \int_0^\tau dt \langle \mathbf{v}_i(0) \bullet \mathbf{v}_i(t) \rangle, \qquad\qquad \text{Eq. 2.23}$$

where $\mathbf{v}(t)$ is the center-of-mass velocity of species i at time t.

A common property used to determine the quality of the electrolytes in this work was cation transference (τ_+). Using D_i evaluated from Eq. 2.22 or 2.23, it was calculated by:

$$\tau_+ = \frac{N_+ D_+}{\sum\limits_{ions} N_i D_i} = \frac{N_+ D_+}{N_+ D_+ + N_- D_-}, \qquad\qquad \text{Eq. 2.24}$$

where N_+ is the number of cations, and the summation in the denominator is over all ionic molecular types.

2.3.3 Radial Distribution Function (RDF)

In statistical mechanics, a radial distribution function (RDF), (or referred as pair correlation function) $g(r)$, is a useful tool to describe the structural characteristic of a system. RDFs describe the probability of finding an atom (or molecule) at distance r from one particular atom (or molecule) compared to the ideal gas distribution.

$$g(r) = \frac{\rho(r)}{\rho^{id}(r)}$$

$$= \frac{\text{average number of particles within a shell between } r \text{ and } r + dr}{\text{number of particles in a ideal gas system}},$$

Eq. 2.25

where the numerator in a fraction indicates the number of atoms at r in the actual system. The denominator gives the number of atoms at r for ideal gas, where $\rho^{id}(r) = N/V$ is the average number density.

According to RDF, the number of atoms in the first coordination shell, called the coordination number (CN), is obtained by taking the integral from the separation distance at which the RDF first increases from zero to the first minimum in $g(r)$ designated as r_{min} by the equation below [117].

$$CN = 4\pi\rho \int_{0}^{r_{min}} g(r)r^2 dr \qquad\qquad \text{Eq. 2.26}$$

2.4   Force Fields

A force field is the form and a set of parameters used in molecular mechanical simulations to describe the potential energy interactions between atoms in a molecular system. Its function and parameters are taken from both experimental work and quantum mechanical calculations in high level. It is a mathematical function that describes how atoms/molecules move, stretch, vibrate, rotate and interact with each other. In the force field function, the presence of electrons is generally ignored.

For the total energy in a force field, a general form can be used:

$$E(\mathbf{r}^N) = E_{bonded} + E_{non-bonded}, \qquad\qquad \text{Eq. 2.27}$$

where $\mathbf{r}^N$ represents the positions of N particles, $E(\mathbf{r}^N)$ indicates the potential energy, it is a function of the positions ($\mathbf{r}$) of N particles (usually atoms).

$$E_{bonded} = E_{bond} + E_{angle} + E_{dihedral} + E_{inversion} \qquad\qquad \text{Eq. 2.28}$$

The force field used for PEO in this research was the transferable potentials for the phase equilibria united atom (TraPPE-UA). It utilizes pseudo-atoms located at the

center of carbon atoms for alkyl groups and treats all other atoms explicitly [118-120], since it treats methyl, methylene, and methane groups as single sites to reduce the number of interaction sites. It has been found to do a good job of reproducing PEO densities over a fairly wide range of temperatures and pressures [118]. This model uses the Lennard-Jones (LJ) interaction potentials of the 12-6 form and fixed electrostatic charges. PEO chains are considered totally flexible with flexible bond lengths, bond angles and dihedrals.

$$E_{bond}(l) = \frac{k_l}{2}(l - l_0)^2,$$

Eq. 2.29

$$E_{angle} = \frac{k_\theta}{2}(\theta - \theta_0)^2,$$

Eq. 2.30

where k_l and k_θ are the force constant; and l_0 is the equilibrium bond length, and θ_0 is the equilibrium bond angle. For all dihedral interactions, a cosine series Optimized Potential for Liquid Simulations (OPLA) form is used:

$$E(\phi) = V_0 + \frac{V_1}{2}(1 + \cos\phi) + \frac{V_2}{2}(1 - \cos 2\phi) + \frac{V_3}{2}(1 + \cos 3\phi),$$

Eq. 2.31

where ϕ is the dihedral angle, and $V_n(n=0, 1, 2, 3)$ are constants. For the pairwise nonbonded interaction energy between two atoms, i and j, which are separated by a distance of r_{ij}, the standard Lennard-Jones (LJ) 12-6 and Coulombic potentials are used:

$$E_{NB}(r_{ij}) = 4\varepsilon_{ij}\left[\left(\frac{\sigma_{ij}}{r_{ij}}\right)^{12} - \left(\frac{\sigma_{ij}}{r_{ij}}\right)^6\right] + f_{ij}\left[\frac{q_i q_j}{4\pi\varepsilon_0 r_{ij}}\right]$$

$$f_{ij} = \begin{cases} 0.5, & \text{if } i,j \text{ are } 1,4; \\ 1, & \text{otherwise} \end{cases},$$

Eq. 2.32

where σ and ε are the LJ the equilibrium distance and well depth respectively, and q_i is the Coulombic charge assigned to atom i. The standard Lorentz-Berthelot combining rules are used for unlike interactions:

$$\sigma_{ij} = \frac{1}{2}(\sigma_{ii} + \sigma_{jj}) \qquad \varepsilon_{ij} = \sqrt{\varepsilon_{ii}\varepsilon_{jj}} .$$

Eq.2.33

A potential truncation of r_{cut} with analytical tail corrections is used for all LJ interactions, and Ewald-summation is used to calculate for long-ranged Coulombic interactions [104].

More complicated force fields also contain other terms, for instance, out-of-plane bending and cross terms. Out-of-plane bending terms can be included into a force field in several ways such as treating it as an "improper" torsion angle which is used for cyclic carbonates. Cross terms reflects linking between the internal coordinates in a force field. Cross terms were found to be useful to predict vibrational spectra, but not all of them were found to be necessary in a molecular mechanics force field to achieve optimal performance [114]. Even more complicated force field terms like "polarization effects" can be included. Polarization interactions are used to describe the molecules' ability to induce dipoles and can improve the transferability of a molecular model. However, they are not used in the described calculations due to the fact that Monte Carlo simulations cannot handle them efficiently, and the very long molecular dynamics simulation time required makes their higher computational expense a major impediment.

CHAPTER 3

THE ADDITION OF PLASTICIZERS IN P(EO)$_{15}$LITFSI ELECTROLYTES

3.1 Introduction

In traditional RLBs, the major safety issue is leakage of liquid electrolytes, which is a serious concern with the toxic and corrosive nature of lithium ions. Furthermore, the liquid carbonate electrolytes can react with the electrodes at high temperatures and in overcharging situations, resulting in fire or explosion [7-11]. One suggested solution, replacing traditional electrolytes with SPEs, is hindered by low ionic conductivity. One common pathway for improvement of SPE conductivity is to introduce plasticizers such as cyclic carbonates shown to enhance the conductivity to be near commercially viable [14, 46, 52, 53, 55, 56]. Plasticized polymers are a compromise between the beneficial properties of solid-state PEs and the high conductivities of liquid electrolytes, but also have, to a lesser degree, the safety issues of liquid electrolytes.

3.2 Simulation Details

3.2.1 Molecular Models

The TraPPE-UA force field was used for PEO (Figure 3.1(a)) [118] and carbonate molecules (Figure 3.1(b) and (c)) [113], which were parameterized to reproduce phase

equilibria. The all-atom force field, developed by Canongia Lopes and co-workers [121], was used for the $N(CF_3SO_2)_2^-$ (TFSI$^-$) ion (Figure 3.1(d)).

(a) Poly(ethylene oxide) (PEO) chain

(b) Propylene Carbonate (PC)

(c) Ethylene Carbonate (EC)
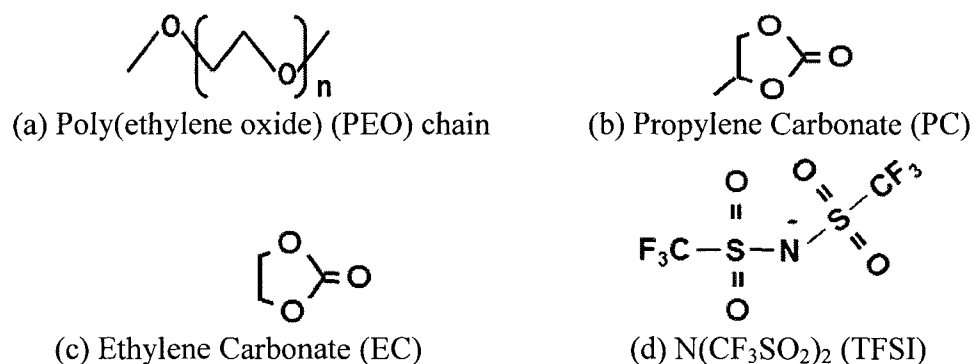
(d) $N(CF_3SO_2)_2$ (TFSI)

Figure 3.1 Molecular Structure for (a) PEO, (b) PC, (c) EC, (d) $N(CF_3SO_2)_2^-$.

While a fixed charge lithium ion force field with Lennard-Jones interactions does exist in the literature [122], a new model was parameterized for this work that better reproduced interactions with dimethyl ether (DME). *Ab initio* results for interactions between lithium and ether oxygens currently exist in the literature, giving a minimum dimer r_{Li-O} distance of 1.8 Å and a binding energy around -38 kcal/mol [123, 124]. We carried out *ab initio* calculations for this dimer using the MP2 level of theory with the frozen core approximation and the Dunning aug-cc-pvtz basis set [125]. The NWChem computational package was utilized for these calculations [126, 127]. The minimum lithium-oxygen dimer distance was 1.82 Å via MP2, and our force field resulted in a value of 1.81 Å, agreeing with *ab initio*. However, the force field gave a binding energy of -30.9 kcal/mol that was weaker than the binding energy from the *ab initio* calculations. The Lennard-Jones parameters for the parameterized Li$^+$ model were $\sigma = 1.4$ Å and $\varepsilon = 0.4$ kcal/mol. The binding energy was possibly not reproduced correctly due to the neglecting of many-body interactions. It should be noted that other force fields exist,

some of which include many-body effects and all-atom models that have been shown to give excellent agreement with experiment for ionic conductivities [123, 128]. Since we desired to perform simulations with fairly high molecular weight polymers in which MC simulations excel at their equilibration, we used a united-atom force field with fixed charges for this work. However, Monte Carlo simulations are ineffective at simulating polarizable molecular models. Furthermore, the long simulation times for the described simulations (which are all 100 ns) may not be suited for our computational resources with many-body effects, which increase the computational expense.

3.2.2 System Parameters

There were three different types of simulation systems investigated in this chapter: one with pure $P(EO)_{15}LiTFSI$ (referred as PURE), one with additional ethylene carbonate (EC), and one with added propylene carbonate (PC). All simulations were set up with four PEO chains with a number-averaged molecular weight (M_n) of 10,000 g/mol with a fixed EO:Li ratio of 15 for the system. In this work, comparisons were made with experimental values with much higher molecular weights (500,000 to 600,000), but the molecular weight's reliance on lithium diffusion has been found to level off around 10,000 g/mol. For example, for a system of PEO with $LiCF_3SO_3$ and fixed an EO:Li ratio of 20:1 at 363 K, at molecular weights of 1000, 10,000, and 100,000 g/mol, the lithium diffusion coefficients (D_{Li}) resulted in 5.0×10^{-7}, 1.0×10^{-7}, and 0.93×10^{-7} cm^2/s, respectively, showing a considerable difference between the 1000 and 10,000 g/mol system of around a factor of five, but only a 7% difference between 10,000 and 100,000 g/mol [129].

For the EC and PC systems, plasticizer was added slowly until it reached 10 wt%, (which will be discussed later). All systems were equilibrated at 1 atm. Two temperatures

were chosen, 348 and 320 K, because the 313 K is the point where PEO-LiTFSI (with EO/Li = 16) begins to crystallize [130, 131], and they allow comparisons with the entire range of temperatures found experimentally [46]. For quantitative agreement with the experiment, it would be better to choose higher temperatures, but the goal of this work is to understand qualitative effects due to the addition of plasticizers.

All systems were placed in a periodic box with a LJ potential truncation of 9 Å employed, with analytical tail corrections. Long-ranged electrostatics were calculated with the Ewald summation technique for the Monte Carlo simulations [104] and the particle mesh Ewald summation technique for the molecular dynamics simulations [132]. This (9 Å LJ cutoff) has been used to model many systems of ions in polar solvents [133-135].

3.2.3 Monte Carlo Simulation Details

In Monte Carlo simulations, all the Li^+ and $TFSI^-$ ions were initially placed on a square lattice, and then four PEO polymer chains were introduced in the system by growing them bead-by-bead using configurational-bias Monte Carlo (CBMC) [136-139]. The configuration of these initial growths which were governed by the first attempt would not be accepted until the whole molecule was grown without overlapping with any neighboring molecules (not the regular Boltzmann acceptance). Following this initiation, the simulations were heated at 100,000 K for a short period of time, then slowly cooled down to 320 K or 348 K, depending on the system to study in the *NVT* ensemble. Following the cooling step, the system was inspected to make sure no salting out occurred, and then simulations were performed in the *NpT* ensemble with an external pressure of 1 atm.

To equilibrate, the types of MC moves in the NpT ensemble were as follows: (a) the standard Metropolis MC translational and rotational moves for all of the molecules [104], (b) volume moves for the equilibration of the pressure of the system, (c) CBMC move for the configuration of $\overline{TFSI}$ and the end segments of PEO, (d) CBMC reptation move for PEO [118], (e) SAFE-CBMC move for the structure of PEO interior segments [140]. Even with these MC moves, the equilibration of polymer structure with an average molecular weight of 10,000 g/mol is not reachable in the system desired, and additional MC moves are required [111]. To efficiently equilibrate long-chained polymer systems, (f) CAMC moves are designed to allow different polymer chains to exchange segments with one another [112, 141]. One of these methods required a certain degree of polydispersity for the polymers, which requires carrying out the simulations in the semi-grand canonical ensemble. This method has been used fairly widely for the investigation of polymers with CAMC simulations [142]. To adjust the required polydispersity, an even distribution of polymer lengths between 75% M_n to 125% M_n was used, keeping the combined PEO molecular weight in the system constantly at 40,000 g/mol. A minimum of 100,000 MC cycles (1 cycle = N × MC moves, where N is the number of molecules in the system) of equilibration were carried out. After 100,000 MC cycles, the system energy and density were examined to make sure that they did not change between adjacent blocks of 20,000 MC cycles.

Simulations with plasticizers introduced were equilibrated by the following method. A liquid phase of EC or PC molecules (depending on the system) were brought into thermal equilibrium with the PEO phase using the GEMC method. The GEMC method uses multiple simulation boxes with no explicit interface, but in thermal contact

[107, 108, 110]. In GEMC, CBMC swap moves are used to equilibrate chemical potential between phases, and volume moves for the equilibration of the volumes of the phases with an outside pressure bath. For our simulations, if allowed to equilibrate completely, the carbonate/PEO ratio would end up being much higher than 10 wt%. Therefore, in order to keep the amount of plasticizer in the PEO phase at the level we desired, no additional swap moves from the carbonate phase into the PEO phase were permitted after the weight percentage reached 10. An additional 50,000 MC cycles of equilibration were carried after this step.

3.2.4 Molecular Dynamics

After equilibration with MC simulation, the coordinates were inputted into a MD simulation along with velocities which were taken from the Boltzmann distribution in order to calculate dynamical properties. A total of 20 ns of equilibration in the NpT ensemble performed at described temperatures (320 or 348 K) and 1 atm. The Berendsen thermostat [143] was used in this step. Following equilibration, 100 ns production runs were carried out in the NVE ensemble to calculate all dynamical and structural properties. After equilibration, the simulation boxes were approximated to 40-43 Å, depending on temperature and composition.

3.3   Results and Discussion

3.3.1   Conductivity (λ)

The present model was intended to design SPEs to have maximized ionic conductivity, an important property for battery operation. To obtain the conductivity, Eq. 2.21 λ times t has to be plotted as a function of t, which should be linear at long enough

times (or as $t \to \infty$). The slope of this linear region is the ionic conductivity. Figure 3.2

gives the plots of $\lambda \times t$ as the function of time for the systems at 320 K.
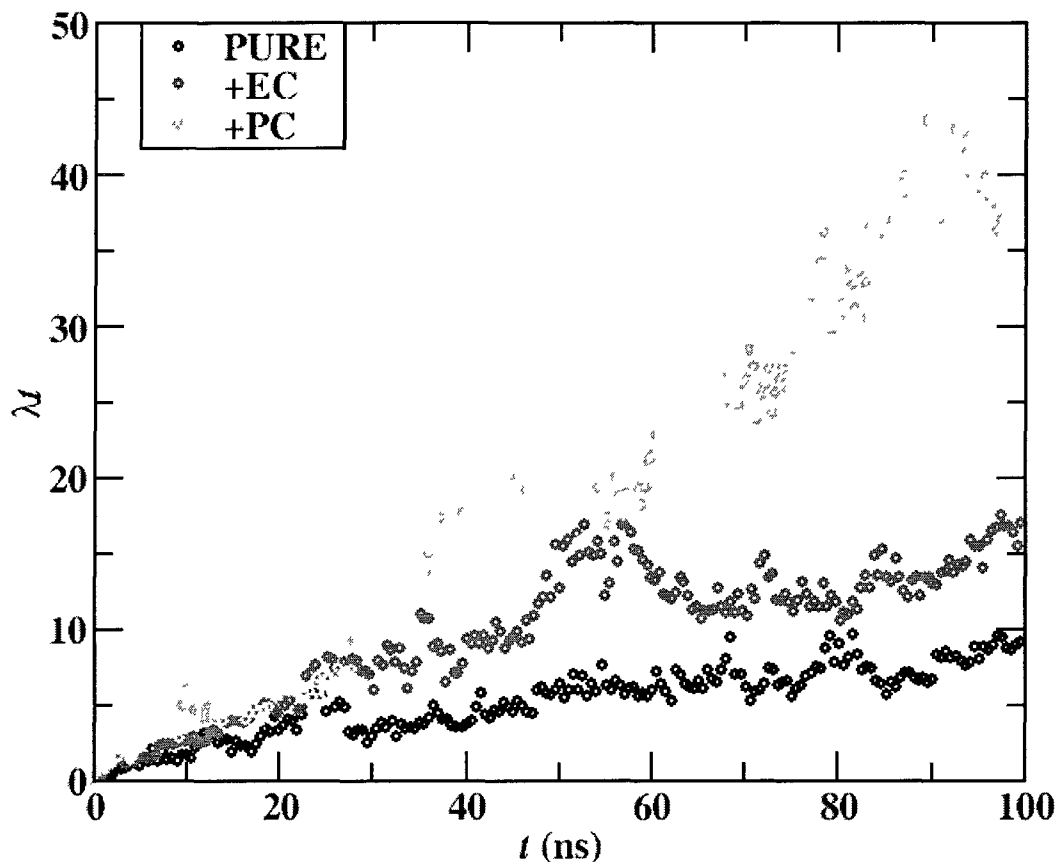
Figure 3.2 Curves used to calculate conductivity for the systems investigated at 320 K

Table 3.1 gives the conductivity calculated for all systems investigated, along

with sets of experimental data. Figure 3.2 shows that the curve used to calculate the

conductivities was somewhat noisy. For the PURE system, the conductivity was found to

stay relatively within a 10% error (via its slope) throughout 100 ns. For with plasticizers,

the conductivity values have an uncertainty of up to 20%.

Table 3.1 Comparison of conductivities (λ) for our simulation results and experiments for the ions and the plasticizers

		T (K)	λ (10^{-4} S/cm)
PURE	Sim.	320	1.78
	Expt.[a]	320	1.40
	Expt.[b]	323	5.00
	Expt.[c]	320	1.80
	Expt.[d]	320	2.33
PURE	Sim.	348	5.40
	Expt.[a]	348	6.31
	Expt.[b]	353	15.1
	Expt.[c]	348	9.50
	Expt.[d]	350	8.52
+PC	Sim.	320	3.92
	Expt.[b]	323	10.20
	Sim.	348	7.28
	Expt.[b]	353	19.50
+EC	Sim.	320	1.62
	Expt.[b]	323	10.96
	Sim.	348	7.87
	Expt.[b]	353	20.40

[a] reference [130] for $(EO)_{10}LiTFSI$; [b] reference [46] for $(EO)_{15}LiTFSI$; [c] reference [144] for $(EO)_{16}LiTFSI$; [d] reference [145] for $(EO)_{20}LiTFSI$

Many experimental values exist in the literature for the conductivity of PEO LiTFSI, but there is only one result for PEO LiTFSI with EC and PC close to our work. For the PURE system, there was a scatter in the experimental data, ranging from 6.31×10^{-4} to 15.1×10^{-4} S/cm. It should be noted that the EO:Li ratio varied from 10 to 20 in these experiments, but there was little correlation between conductivities and EO:Li in this range. For example, a previous study of a conductivity versus EO:Li ratio for an isotherm at 333 K of PEO LiTFSI showed only a small change in the conductivity ranging between 5×10^{-4} and 7×10^{-4} throughout the block of 12-24 EO:Li ratio [129]. The record of the experimental data shown in Table 3.1 is much larger than that, so the values probably depend on the experimental procedure and sample history [145]. The

simulation results are less than the values in comparison to the experiment for the PURE system but appear to be within a factor of two of the experimental range. It has been argued that the conductivity will increase if including polarizability in the molecular models [123]. Since our models did not include polarizability this factor might be the hidden reason for the conductivity being lower than the experiment. Nevertheless, the simulation results presented here are reasonable, as the simulation results are within the range of experimental data, toward the lower end at 320 K. In addition, from 348 to 320 K, the reduction in conductivity is consistent between simulations and experiments, for reduction of the experiments decreasing from 81% to 67%, and for the simulations, the reduction is 67%.

With the addition of plasticizers, the conductivities increase by 35% for PC and 45% for EC for the simulation at 348 K. Obviously, these results gave the expected behavior of enhanced conductivity with the addition of plasticizers. The corresponding values for the experiment were 29% for PC and 46% for EC [46]. Even though the absolute values do not agree with the data from this experiment, the consistency between the two temperatures was excellent, showing strong qualitative agreement.

3.3.2 Diffusion (D) and Lithium Transference (τ_+)

Using Eq. 2.22, Figure 3.3 gives the $<MSD(t)>$ as a function of time from the simulations at 320 K. It can be observed that the curves are fairly linear after around 20 ns of simulation time. For the PURE system, the simulation times were extended 100-200 ns and were found to have the same slope as the previous 100 ns within the error of the calculation (results not shown). Apparently, it takes the system around 20 ns before the *MSD*s increase in a linear fashion, and beyond that, the *MSD*s appear to be fairly well behaved. These curves show a degree of noise not found in other simulation results [123],

but due to the lower temperatures used here (and overall lower values in *MSD*), our results were expected to be noisier.
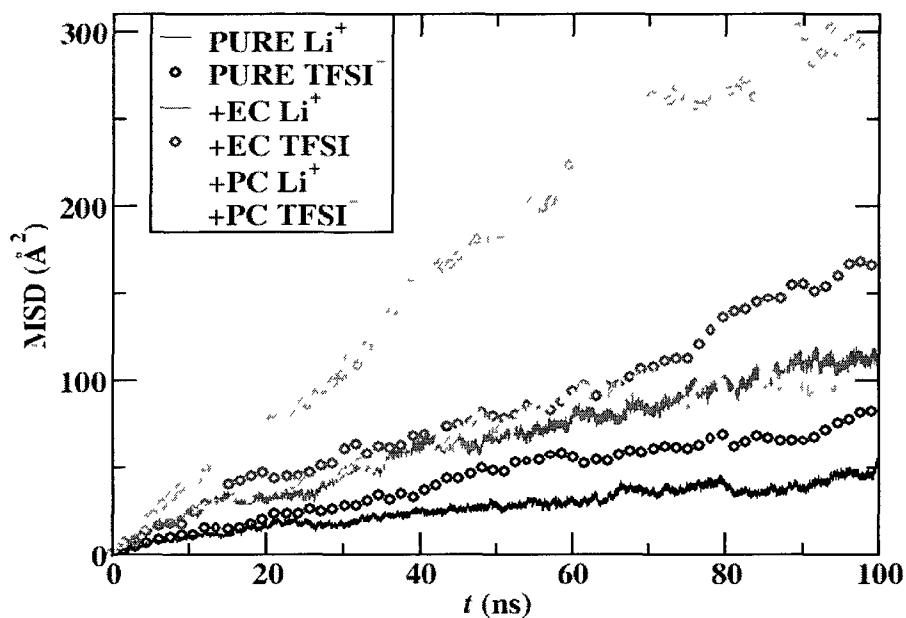
Figure 3.3 *MSD*s of cations and anions for the systems investigated at 320 K

A common property calculated to determine the quality of the electrolytes is lithium transference (τ_+). It was calculated by Eq. 2.24, since the numbers of cations and anions are equal, the equation yields to,

$$\tau_+ = \frac{N_+ D_+}{\sum_{ions} N_i D_i} = \frac{D_+}{D_+ + D_-}.$$

Eq. 3.1

A higher lithium transference is often desirable for RLBs since lithium can only be oxidized/reduced at electrodes, so the higher the transference number, the higher the efficiency and capacity of the battery. The values of D_i and τ_+ are shown in Table 3.2, along with experimental values for comparison. The uncertainties in the diffusion coefficients were estimated via their slopes to be around 10%.

Table 3.2 Comparison of τ_+ and D for simulations results and experiments for the ions and the plasticizers

System		T (K)	τ_+	$D(10^{-8}\ cm^2\ s^{-1})$		
				Li^+	TFSI	Plast.
Pure	sim.	320	0.50	1.93	1.87	---
	sim.	348	0.337	3.10	6.10	---
	expt.[a]	348	0.487	14.2	14.9	---
+PC	sim.	320	0.252	1.91	5.68	24.9
	sim.	348	0.239	3.93	12.5	82.7
	expt.[a]	348	0.262	12.6	24.6	---
+EC	sim.	320	0.406	1.81	2.55	21.6
	sim.	348	0.300	3.65	8.51	55.5
	expt.[a]	348	0.381	17.2	25.3	---

[a] reference [46] for $(EO)_{15}LiTFSI$

We could not find experimental values for a system with an EO:Li ratio of 15 at 320 K. It should be noted that the experimental values were based on an approximation of an ideal dilute solution, so they may not be quantitatively accurate [46] yet should hold quite strongly for qualitative trends. No uncertainties were found in the experimental results, but similar measurements were made of $P(EO)_{16}LiTFSI$ at 358 K and gave a value τ_+ of approximately 0.41 ± 0.08 [146]. This number is at a higher temperature than the one simulated in this work but provides a good baseline of the uncertainty and spread expected from the measurements. Even though the simulation results were lower than the experiment, this difference is consistent throughout the range of systems investigated. For instance, the addition of plasticizers decreased τ_+, with the PC system showing the largest τ_+ decrease. It is interesting that when PC was added to the system, lithium diffusion stayed relatively unchanged, and the $TFSI^-$ diffusion increased more significantly. At the lower temperature of 320 K, the addition of plasticizers actually decreased lithium diffusion, while increasing $TFSI^-$ diffusion for both plasticizers. Also, the $TFSI^-$ diffusion increased to a greater degree for the PC system than the EC system. From these results, it

is apparent that the addition of EC or PC plasticizers at this level may have little benefit for RLBs as most of the conductivity enhancements appear to be due to the anion, which is not what is oxidized and reduced at the electrodes. This result was somewhat unexpected, as the diffusion coefficients for the plasticizers are much higher than any of the ionic species themselves (Table 3.2), by over ten times the magnitude in many cases. If it would be possible for a lithium ion to strongly bind with one of the carbonates, it may have the power to travel faster as a complex due to a vehicle mechanism, but this does not appear to be the case. In addition to the polymer system, the diffusion coefficients and degree of dissociation (DOD), which is the fraction of original solute molecules that have dissociated, for LiTFSI in pure PC and EC were calculated using the described models, and the results are given in Table 3.3.

Table 3.3 Comparison of conductivities, diffusion coefficients, and degree of dissociation (DOD) for the ions LiTFSI and EC or PC

System		T (K)	λ (10^{-3} S/cm)	D (10^{-6} cm^2/s)		DOD
				Li$^+$	TFSI	
EC	Sim	313	5.1	1.0	1.3	0.64
	expt[a]	313	8.3	2.1	3.1	N/A
PC	Sim	303	2.1	0.4	0.5	0.72
	expt[a]	303	5.2	1.6	2.1	0.62

[a] reference [146]

The diffusion coefficients were smaller than the experiment by around a factor of two to four, while the ionic conductivities were around a factor of two lower than the experiment, consistent with the results for LiTFSI motion in the polymers. As was discussed for ionic conductivity in PEO-LiTFSI, the non-polarizability was the likely reason the ionic diffusion was lower than experiment. If the quantitative agreement with the experiment is desired, using more computationally expensive polarizable models is

probably necessary because the previous works with polarizable models have found better agreement for diffusion coefficients [123, 128]. The DOD of LiTFSI is given in Table 3.3 for EC and PC and shows somewhat higher DODs than listed experimentally for PC.

3.3.3 Structure

The structure of the system was investigated by calculating radial distribution functions (RDFs) of lithium with all oxygens with which it had significant binding. The RDFs between lithium and the oxygens for the systems investigated at 320 K are given in Figure 3.4, taken from Eq. 2.25. Besides the paired atoms shown in Figure 3.4, lithium did not show significant binding with any other. For instance, lithium did not coordinate with the sp^3 carbonyl oxygen (that is, bonded to two carbons) or the nitrogen atom in $TFSI^-$.
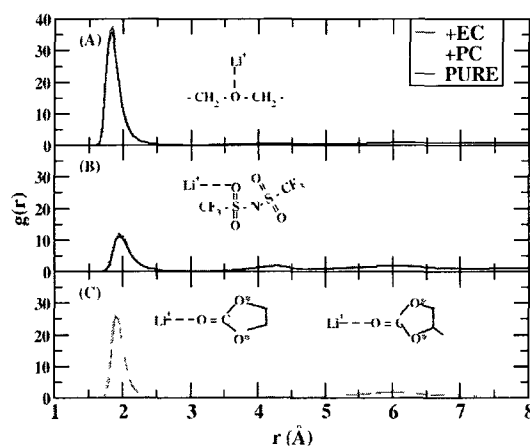
Figure 3.4 RDF at 320 K for lithium with (A) EO oxygens,
(B) TFSI oxygens, (C) carbonate oxygens

The strongest binding of lithium was with EO oxygens, the secondary binding was with carbonate oxygens, and weakest with the $TFSI^-$ oxygens, as evidenced by the RDF peak height. This phenomenon explains why the lithium diffusion does not change

significantly in the addition of plasticizers because of the relatively modest concentrations of plasticizers in the system, only ten weight percent, EO oxygens are still governing, and the addition of binding carbonate oxygens in the EC and PC systems is too weak to change the lithium–ether oxygen binding.

The average first Li-O(EO) RDF peak is located at a distance of 1.85 Å. The coordination number (CN) can be obtained by integrating the RDF with the number density over this first peak (up to 2.5 Å) using Eq. 2.26. For the PURE system at 320 K, the Li^+ has a CN of 4.8 EO oxygens and 0.5 $TFSI^-$ oxygens, giving a total of 5.3. This coordination number has shown a good agreement for a more concentrated salt system with an EO:Li = 7.5, in which a CN of 4.9 ± 0.5 was found [147]. With the addition of plasticizers, little change in the distance or positions of Li-EO RDF peak can be observed. However, with the addition of PC, lithium binds to a greater degree with the $TFSI^-$ oxygen, showing that PC may actually induce stronger interactions between lithium and $TFSI^-$. Multiple 20 ns blocks of simulations were compared to make sure that this result was not due to statistical noise, and in all comparisons, the Li-O(TFSI) increased with the addition of PC. What was somewhat unexpected was that the addition of EC has little to no effect on the Li-O(TFSI) RDF, while PC does.

Figure 3.5 gives the RDF for carbonate oxygens with $TFSI^-$ oxygens and for EO oxygens with EO methylene groups. Interestingly, the PC oxygen appeared to show a significant degree of binding with $TFSI^-$ oxygens (with a lithium ion bridging them), while EC oxygens showed very little binding with these. The EO-EO oxygen-oxygen RDF shows stronger binding for PC system and similar binding in the PURE and EC systems.
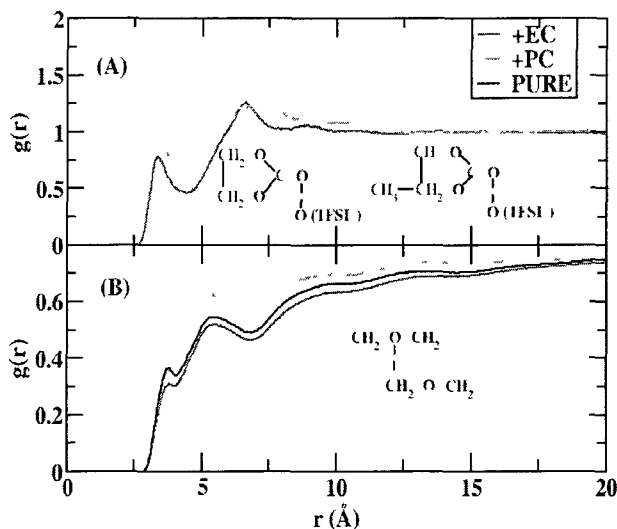
Figure 3.5 RDF at 320 K for (A) carbonate oxygens with TFSI oxygens,
and (B) EO oxgyens with EO methyl groups

A snapshot representative cluster from the PC system at 320 K is shown in Figure

3.6, in which a single lithium ion and all non-PEO species (including PC and TFSI)

bound with it are shown. PC binding with the lithium atom appears to induce interactions

between lithium and TFSI⁻.
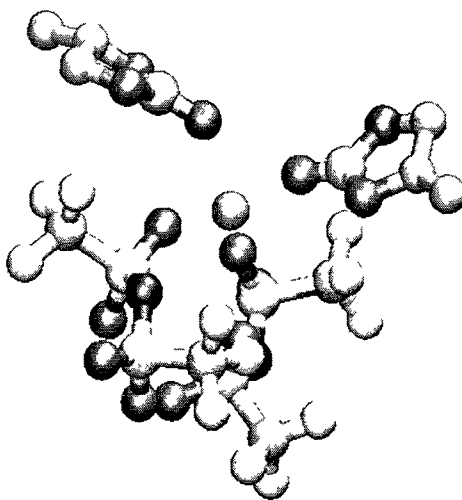
Figure 3.6 Snapshot of a cluster of molecules bound with the lithium ion,
including two PCs and one TFSI⁻ molecules

This binding is the origin of the higher first peak showed in the RDF between the PC and TFSI⁻ oxygen. The methyl group in PC did not show any significant binding with any TFSI⁻ atoms, with no high first RDF peaks between the atoms (not shown). However, the shape of PC appeared to have a small effect on the ability of the systems to form clusters of this type. This effect is evident in the RDFs, since EO group bind the strongest in the PC system, and PC and TFSI⁻ oxygens showed a higher first peak due to their mutual binding with a lithium ion. Apparently, the methyl group in PC allowed the formation of a structure in which clusters of lithium, PC, and TFSI⁻ were embedded in the PEO. This structure is probably why the TFSI⁻ diffusion increased to a greater degree in the PC system than the EC system. In contrast, the increase in lithium diffusion was very small due to binding with TFSI⁻ and PC, showing that there were a significant number of bounded lithium ions in the environment with slow diffusion.

Table 3.4 gives the coordination number (*CN*) of different oxygen species with lithium ions for the systems investigated at 320 K. The reason for the rather small impact of the addition of plasticizers to lithium diffusion can be understood by the *CN*s, as lithium rarely coordinates with the carbonate oxygen, even though there are over twice as many PEO oxygens as carbonate oxygens. The addition of plasticizers increases the *CN* of TFSI⁻ oxygen, especially with the addition of PC, as described previously. Taken as a whole, though, the binding of the carbonates was not strong enough with lithium to have a large effect on lithium diffusion.

Table 3.4 Oxygen *CN* per lithium ion at 320 K

System	Li-O(EO)	Li-O(TFSI)	Li-O(C=O)	Total
PURE	4.84	0.59	---	5.43
EC	4.60	0.65	0.15	5.41
PC	4.43	0.69	0.18	5.30

3.3.4 Lithium Residence Times (ACF)

There are two mechanisms that can be considered to contribute in the total Lithium ion transport: one is lithium ion motion along PEO, hopping from one oxygen to the other; the other is the mechanism that lithium bonding with either a plasticizer or an anion. To better understand what the effect of introduction of plasticizers on these mechanisms was, the lithium residence time is helpful. The residence time was calculated for lithium with each kind of oxygen it was strongly bind with. To calculate the residence times, a time autocorrelation function (ACF) was used:

$$C_{Li-O}(t) = \frac{\langle H_{ij}(t) \times H_{ij}(0) \rangle}{\langle H_{ij}(0) \times H_{ij}(0) \rangle},$$

Eq. 3.2

where $C_{Li-O}(t)$ denotes the ACF value; $H_{ij}(t)$ is one if ith Li$^+$ is coordinated with jth oxygen atom, such as a special EO unit, and zero otherwise.

The distance to the first coordinate shell was 2.5 Å, taken from Li-O RDF peaks. The ACF value as a function of time is given in Figure 3.7 on a logarithmic scale.
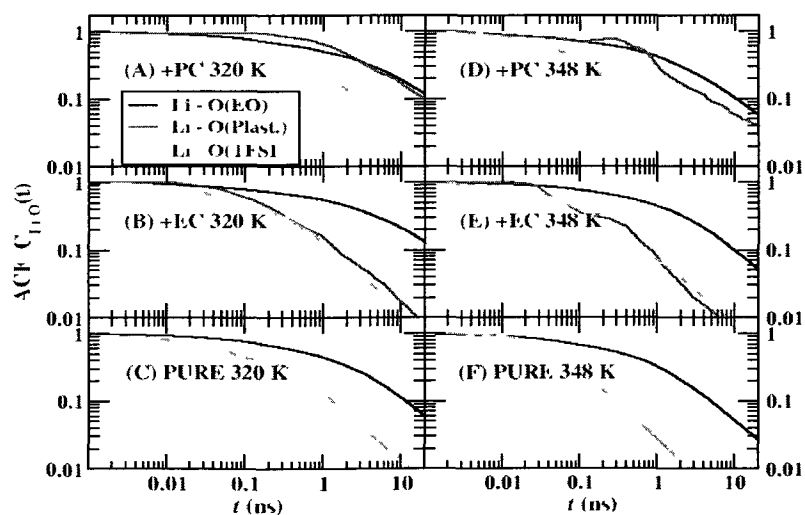
Figure 3.7 Residence time ACFs of Li$^+$ moving along PEO, EC/PC, and TFSI$^-$ for all simulations

For PURE systems, it appeared that the longest lithium binding was with an EO oxygen, which was expected. With the addition of EC, lithium appeared to have a similar degree of binding with EC oxygens and with TFSI$^-$ oxygens, having its ACFs falling off much faster than with an EO oxygen. For addition of PC system, lithium binding with PC more closely followed the ACF of EO oxygens, and its ACF dropped off much slower than with TFSI$^-$. By fitting ACFs to $\exp[-(t/\tau_{res})^{\beta}]$, where β and τ_{res} were fitted valuables, the mean residence times, τ_{res}, were evaluated. The results are given in Figure 3.8. The value of β ranged from 0.3 to 0.5.
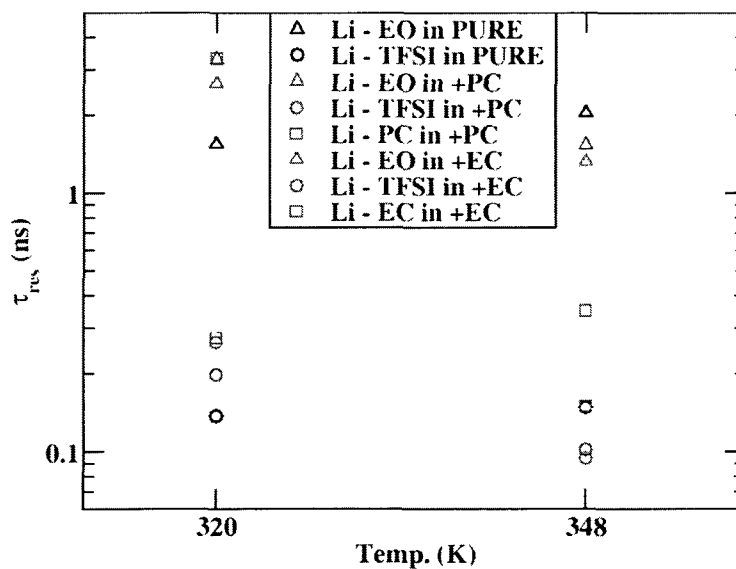
Figure 3.8 Comparison of total residence times of Li$^+$ with oxygens of EO, TFSI$^-$, and plasticizer (EC or PC) for all systems investigated

In sequence of residence time, from the longest to the shortest, we observed is with the EO oxygens, with EC and PC oxygens , and then with TFSI$^-$ oxygens for all cases. The longest τ_{res} of the EC and PC oxygens is with PC oxygens. With the addition of PC at 320 K, the residence time of lithium binding with PC has a similar residence time as EO, which is the one exception to this trend. This result was consistent with the

ACF behavior that can be observed in Figure 3.6. Interestingly, the addition of plasticizers influenced the τ_{res} values for Li-O(EO), increasing τ_{res} at 320 K and decreasing them at 348 K. This result is consistent with the lithium diffusion results calculated for the two temperatures, in which $D_{Li}+$ decreases at 320 K but increases at 348 K with addition of plasticizers.

Clearly, the EO oxygens are the species with which lithium most strongly binds, and altering this binding is what mostly promotes lithium mobility. The strongest effect the addition of plasticizers have on the systems appears to be how they influence lithium binding with EO oxygens, with shorter residence time values after the addition of plasticizers at the higher temperature and longer residence values at the lower temperature. This result is consistent with the lithium diffusion results calculated for the two temperatures, in which lithium diffusion increases at 348 K with the addition of plasticizers but decreases at 320 K.

3.3.5 Mechanism of Lithium Transport

To better understand the mechanism for lithium transport, the probability for a lithium ion to bind with one oxygen while bound to another was investigated. The hopping probability is given as follows:

$$P(O_i - O_j) = \frac{N_{ij}}{\sum_i N_i}, \qquad \text{Eq. 3.3}$$

where N_{ij} is the number of cases where a lithium bound with oxygen i begins to bind with oxygen j, and $N_i = \sum_j N_{ij}$ are the total number of times when a lithium bond with an oxygen of type i begins to bind with any other oxygen. The definition for binding is when the lithium-oxygen distance is less than 2.5 Å. This hopping probability will be skewed to

represent j oxygens that are the most concentrated in the system, the EO oxygens. To correct for this, we weighted the hopping probability by the ratio of oxygens of type j over all oxygens in the system.

$$W(O_i - O_j) = \frac{P(O_i - O_j)}{N_j / \sum_k N_k},$$

Eq. 3.4

where N_j represents the number of oxygens of type j in the system and $N_j = \sum_i N_{ij}$; and k indicates the number of oxygens in the system. It should be noted that there are four oxygens per TFSI$^-$ ion, one per PEO repeat unit, and one per PC or EC (as only the carbonyl oxygen showed any binding).

Figure 3.9 gives $W(O_i\text{-}O_j)$ where O_i is an EO oxygen. It shows jumps to adjacent EO oxygens (including those in another PEO chain), to carbonyl oxygens, and to TFSI$^-$ oxygens. Of interest is that it was very rare for a lithium ion to jump to a nonadjacent PEO oxygen. This figure show that the primary mechanism for movement along a PEO chain was along its longitudinal direction, even in an amorphous system.
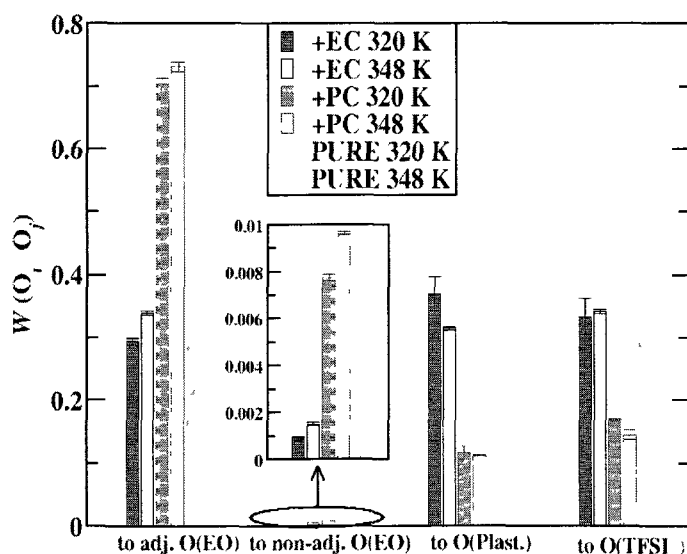
Figure 3.9 $W(O_i\text{-}O_j)$ for the systems investigated, where O_i is an EO oxygen

With the addition of EC or PC, the probability to move to a TFSI⁻ oxygen was reduced, which was expected, as the RDFs show stronger interactions with the carbonate oxygen than with a TFSI⁻ oxygen. The jump probability to another PEO oxygen, though, increased dramatically with the addition of PC. This phenomenon was not observed with the addition of EC. This result was not expected as the PC system has a higher first TDF peak for lithium with the TFSI⁻ oxygen, and one would think that jumps to TFSI⁻ oxygen would increase. However, this result was consistent with the description given with the RDFs and the snapshot (Figure 3.6). If clusters with lithium in the center are formed in the PC systems, then it would be more difficult for a lithium ion bound to a PEO chain to transfer to a carbonate or TFSI⁻ oxygen, since they will not be in as close of a proximity.

Figure 3.10 shows the jump probability for lithium from a TFSI⁻ oxygen to other possible oxygens. The most probable transfer of the lithium ion is to another TFSI⁻ oxygen, on either the same molecule or a different one.
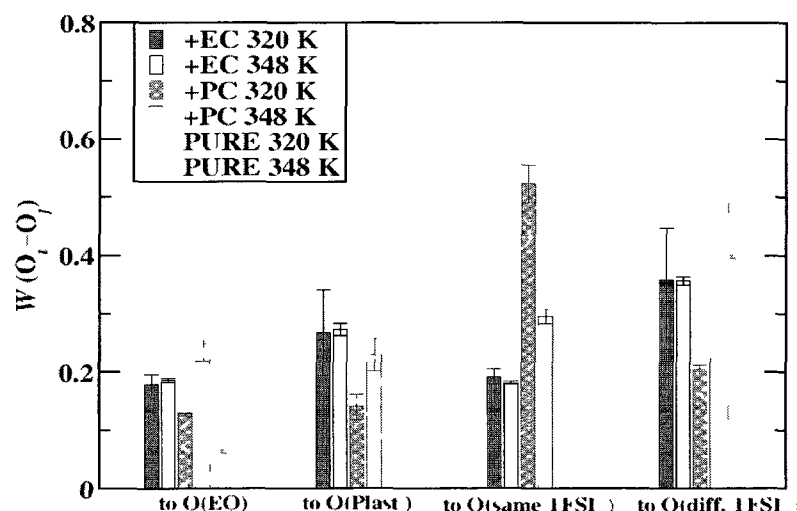
Figure 3.10 $W(O_i\text{-}O_j)$ for the systems investigated, where O_i is a TFSI⁻ oxygen

The addition of plasticizers decreased the probability to transfer to TFSI⁻ oxygens

of a different molecule and also decreased the probability of transferring to an EO oxygen.

PC had the most pronounced effect, by promoting transfers between TFSI⁻ oxygens on

the same molecule. This result was somewhat expected, as the addition of PC promotes

stronger binding between lithium and TFSI⁻ oxygens, as shown in the RDFs.

Figure 3.11 shows the jump probability for a lithium from a carbonate oxygen to

another oxygen. The PC system again showed the highest probability to jump to a TFSI⁻

oxygen, which was consistent with the previous results. The EC system showed differing

behaviors, depending on the temperature of the system. At 320 K, the lithium jump

probability was similar to all three oxygen types. At 348 K, lithiums were most likely to

jump to another EC oxygen. In general, the addition of PC enhances lithium binding with

TFSI⁻ oxygens, and the probability to jump to one, which was not observed with the

addition of EC to nearly the same degree.
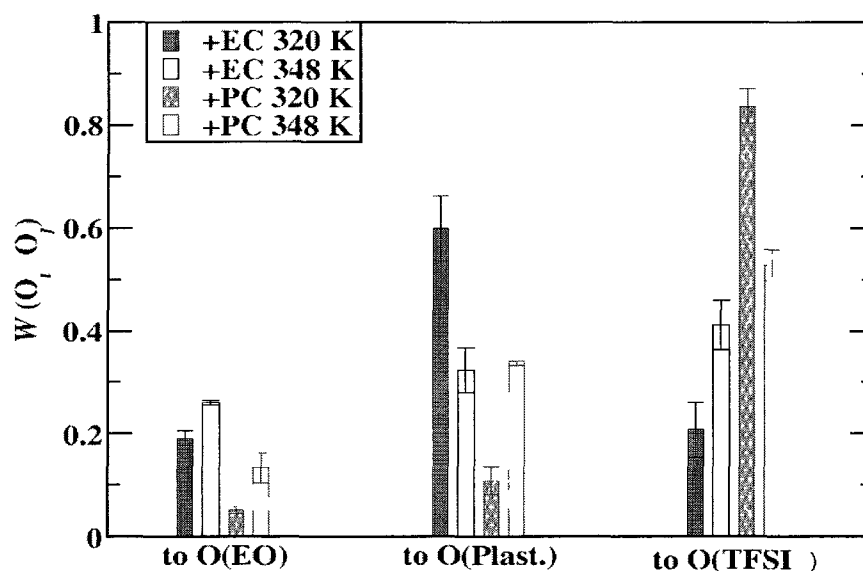
Figure 3.11 $W(O_i\text{-}O_j)$ for the systems investigated, where O_i is a carbonyl oxygen

3.3.6   Effect of Environment on Lithium Diffusion

The diffusion coefficients of lithium when bound to different oxygens defined as within a distance of 2.5 Å are shown in Figure 3.12. The diffusion coefficients were *not* calculated from 100 ns trajectories, but of much shorter 5 ns trajectories. Clearly 5 nanosecond is too short of a time to estimate the true diffusion coefficient, but in general, fewer than 50% of the lithium-oxygen binding events lasted longer than 5 ns. As a result, 5 ns was chosen to get reasonable sampling and to allow *qualitative* comparisons to be made in diffusion coefficients.
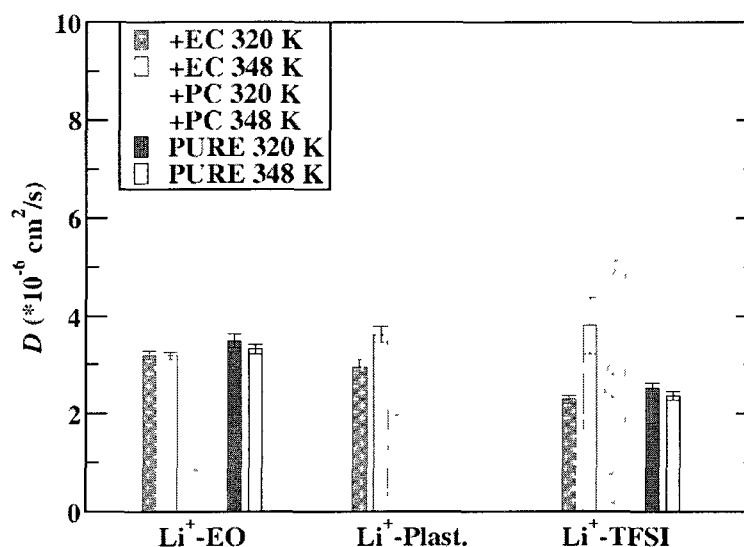
Figure 3.12 Diffusion coefficients for lithium when bonded to different oxygens

The Li^+-EO values represent lithiums that were only bound to EO oxygens, while for plasticizer and $TFSI^-$ oxygens, the values are for lithium ions that were bound to them but can also be bound to other oxygens as well. This value was done because the vast majority of lithium ions were bound to at least one EO oxygen. In examining the lithium ions bound to EO oxygens, it can be observed that the addition of PC slightly

increases the diffusion of these oxygens, but the addition of EC had little effect. What is very interesting is that lithium ions bound to plasticizers did not show a significant increase in diffusion and actually showed a noticeable decrease for the PC system at 320 K. It should be noted that lithiums bound to plasticizers were almost always bound to EO oxygens as well, and the slower lithium diffusion was probably due to a cooperative defect between the PC and EO oxygens. For cases when lithium was bound with a TFSI⁻ oxygen, unexpected results occurred. In the PURE system, lithiums bound to TFSI⁻ oxygens diffused more slowly than other two systems while in the EC system, lithiums bound to TFSI⁻ oxygens diffused more slowly than other two systems at 320 K and about the same, within the standard error, at 348 K. In contrast, for the PC system, lithium ions bound to TFSI⁻ oxygens had much higher diffusion than in the other cases. This result was expected, as for the PC system only, TFSI⁻ diffusion was increased significantly, and it would be expected that lithiums bound with them would also have faster diffusion. This result also brings some insight into how best to optimize lithium diffusion. For the case of LiTFSI, the binding of lithium with TFSI⁻ is not very strong, so plasticizers needed to bind strongly with lithium itself to facilitate faster diffusion. If another anion that binds stronger with lithium were used, enhancing the anion diffusion should additionally enhance the lithium diffusion so well.

3.4   Conclusions

Molecular dynamics simulations, aided by connectivity-altering Monte Carlo simulations for equilibration, were used to understand how the addition of carbonate plasticizers influences ionic conduction and lithium transference for polymer electrolytes of LiTFSI in poly(ethylene oxide) with a number-averaged molecular weight of 10,000

g/mol. The results showed increases in ionic conductivity with addition of plasticizers, but fairly little increases in lithium diffusion, pointing to faster TFSI anion diffusion as the main reason for the higher conductivity. The addition of propylene carbonate appeared to create domains that included clusters of propylene carbonate, lithium, and TFSI ions. These domains increased the diffusion coefficient of TFSI anion, but also enhanced the binding between lithium and TFSI oxygens, causing small increases in lithium diffusion. Future avenues for enhancing lithium diffusion in polymer electrolytes may focus on finding molecules that bind more strongly with lithium and allow the formation of faster moving cluster.

CHAPTER 4

THE ADDITION OF NANOPOROUS FILLERS IN
P(EO)$_{15}$LICLO$_4$ ELECTROLYTES

4.1   Introduction

The development of novel SPEs remains as an increased interest due to their high

safety and reliability in the last few decades [148]. Among the polymeric material

reported, PEO-LiX (X=ClO$_4^-$, TFSI$^-$, etc.) electrolytes are the most commonly studied [2,

149-151]. For vehicle operations, the electrolyte needs to have good conductivity at low

temperatures, but the ionic conductivity of PEO-LiX complexes only reach useful values

at high temperatures. This low ionic conductivity is due to the fact that PEO-LiX

crystallizes at low temperatures. Multiple approaches have been studied to improve the

conductivity and to lower the operation temperatures of PEO-LiX polymer electrolytes to

near ambient temperatures. Recently, it has been reported that the addition of nanoporous

membranes such as TiO$_2$, Al$_2$O$_3$ or SiO$_2$ to PEO-LiX polymers enhances its ionic

conductivity [75, 76, 78-80, 152]. Some of those previous works conjectured that

increasing both the interaction strength between the porous materials and PEO increases

the overall ionic conductivity in PEO-LiX.

4.2   Simulation Details

4.2.1   Molecular Mode

The transferable potentials for phase equilibria united-atom (TraPPE-UA) force field was used for PEO [118-120], which has been shown to be good for reproducing the structural properties of high molecular weight PEO over a wide range of temperatures and pressures [118, 153]. The all-atom ClO_4^- force field, developed by Baaden, M. et al. [154], was used. A lithium ion force field was parameterized to give a reasonable binding energy and configuration with dimethyl ether (DME) in comparison with *ab initio* calculations as shown in Table 4.1 and described in the previous chapter and the parameters for the lithium ion are also listed in Table 4.2. The Dreiding force field was utilized for aluminum [155]. The Alumina intramolecular interactions were taken from G. Gutierrez and B. Johansson [156].

Table 4.1 *Ab initio* results for interactions between alumina and $EO/Li^+/ClO_4^-$

System	$r_{ab\ initio}$ (Å)	$U_{ab\ initio}$	r_{model}	U_{model}
Li^+-O(H)	1.81	-64.1	1.80	-58.2
O_{DME}-O(H)	2.83	-4.53	2.83	-4.32
$O(ClO_4)$-O(H)	2.76	N/A	2.83	-37.4
$O(ClO_4)$-Al	1.93	N/A	2.00	-37.4
Li^+-O(EO)	1.82	-38.0	1.81	-30.9

Table 4.2 LJ parameters for the parameterized atom model used

	σ (Å)	ε (kcal/mol)
Li	1.4	0.4
O(H)	3.48	0.1
O(Al only)	2.95	0.1
H	1.00	0.0

For interactions between the alumina and the polymer/lithium/ClO_4^-, we carried out DFT B3LYP calculations with the aug-cc-pvdz basis set to parameterize them. Table 4.1 gives the *ab initio* results for interactions between alumina and EO/Li^+. In general, there was good agreement between the force field and the *ab initio* results for the geometries, but the binding energies were generally lower than the *ab initio* results. However, there was a degree of consistency between the different results. The Lennard-Jones parameters for the parameterized atoms model used are shown in Table 4.2.

4.2.2 System Parameters

There were three different types of systems investigated in the work described in this chapter. One was including only PEO chains with $LiClO_4$ (BULK); the other two had a slab of aluminum oxide (SOLIDs), one with hydroxyl terminated groups to mimic the acid treated alumina surface (ACIDIC) (Figure 4.1(a)), and the other with oxygen terminal groups to mimic the basic treated surface (BASIC) (Figure 4.1(b)).

(a) Acidic System (b) Basic System
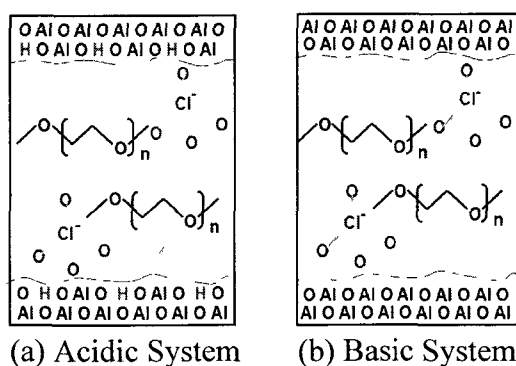
Figure 4.1 Schematic of the SOLID systems investigated.
(a) Acidic system, (b) Basic system

Each system had four PEO chains with a number-averaged molecular weight (M_n) of 10,000 g/mol and the ratio of EO:Li = 15:1. In this work, a comparison was made with the experimental values with a number-averaged molecular weight of 2×10^6 g/mol, and

with a ratio of EO:Li=16:1 [157], but the molecular weight dependence on the lithium diffusion has been found to level off around 10,000 g/mol [129] as we mentioned in our previous work [153].

Nanoporous alumina which has evenly sized pores with an average diameter of 10 nm can be fabricated. These types of pores have already been proposed for use as separators for liquid electrolytes [158]. In our work, a surface of amorphous alumina instead of a pore was simulated. While one to one comparisons with an experiment is not possible, qualitative comparisons can be made, such as how the acidic surface versus basic surfaces influence ionic conductivity. We specifically investigated how the surface groups influenced PEO and LiX structure and dynamics.

For the SOLID systems, a soft wall was introduced with a repulsive potential of the form A/r^{12} with A=100 kcal/mol on each side. The wall itself had a length of 4 nm to represent the width of the alumina surface used. After an initial equilibration period as described in Section 4.2.3, the soft wall was replaced with a 4 nm slab of amorphous alumina, either ACIDIC or BASIC. All the systems had periodic boundaries and minimum image convention with LJ cutoff of 12 Å and analytical tail corrections. Long-ranged electrostatics were calculated by the Ewald summation technique for MC simulations [104] and the particle mesh Ewald summation technique for the MD simulations [132]. Three different temperatures were simulated and compared with experiment: 323 K, which is the eutectic temperature of PEO-LiClO$_4$, 348 K, and 373 K.

4.2.3 Monte Carlo Simulation Details

The simulation detail of BULK system is similar to the PURE system in Section 3.2, and further elaboration is not given here. The simulations with the addition of a slab of aluminum oxide were equilibrated by a multistep simulation strategy: (1) MC

simulations were all started out with a soft surface solid (with A/r^{12} repulsion) to represent alumina as described in the previous section. (2) MC simulations were run at a relatively high temperature (500 K) to equilibrate PEO with $LiClO_4$, in which $LiClO_4$ had their charges reduced by 90%. In this step, the densities of PEO and $LiClO_4$ were checked to see if they are uniform. (3) The soft surface was replaced with an amorphous alumina slab, either ACIDIC or BASIC. This amorphous alumina slab was originally annealed at 2000 K for 10 ns via MD simulations, and cooled to 500 K. (4) Further MC simulations at 1 atm and their respective temperature were carried out to equilibrate the systems further. (5) MD simulations were then spawned, followed by 100 ns of equilibration, and at least 200 ns of production.

4.2.4 Molecular Dynamics Simulation Details

After equilibration with MC simulations, the lengths of simulation boxes were approximately $40{\times}40{\times}40$ $Å^3$ for BULK, and $140{\times}27{\times}27$ $Å^3$ for SOLID systems, in which approximately 40 Å was alumina. The Boltzmann distribution was used to initialize the velocities, along with the coordinates taken from the MC simulations. The time step used in all MD simulations was set to 1 fs.

4.2.4.1 Diffusion and transference parallel to an interface

Diffusion is a basic property and the ability to evaluate it in a confined region is necessary for a complete understanding of the dynamics in an interfacial region. The principal process of ion transport in solid-fluid interfacial regions is very important for a variety of chemical systems [159-161]. For the determination of diffusion coefficients parallel to a solid-polymer interface $D_{//}$ in individual slabs, 10 Å along the z-direction, showing in Figure 4.2. A previously developed method [162, 163] was used to calculate these values, a brief overview is shown in Figure 4.2.
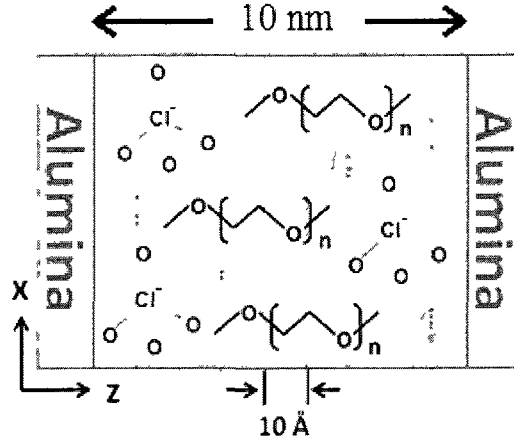
Figure 4.2 Schematic of the system that was modeled using a molecular simulation. It should be noted that the system is periodic

First, we calculated the survival probability $P(\tau)$ for each ion to stay within a certain region ($\mathbf{R}_k$) for the time interval $(0,\tau)$,

$$P_i(\tau) = \frac{N_i(0,\tau)}{N_i(0)},$$

Eq. 4.1

here $N_i(0)$ indicates the number of ions i, Li^+ or ClO_4^-, which originate in a certain region at the beginning of the time interval, $N_i(0,\tau)$ indicates the number of ions which stay within the region for the entirety of the time interval, if it leaves the region for even one time step, it is not counted.

Next, the *MSD*s of the ion i that stay within a specified region $\mathbf{R}_k$ for the entirety of time interval can be determined

$$\left\langle \Delta\mathbf{r}(\tau)^2 \right\rangle_{\mathbf{R}_k} = \frac{1}{N_i(0)} \sum_{i \in \mathbf{R}_k} [\mathbf{r}_i(\tau) - \mathbf{r}_i(0)]^2 .$$

Eq. 4.2

Finally, by using the Einstein relation for long time intervals $(\tau \to \infty)$, the diffusion coefficient parallel to an interface, $D_{//} = D_{xy}$ in our case, can be calculated below:

$$D_{//} = D_i^{xy}(\mathbf{R}_k) = \frac{\left\langle \Delta \mathbf{r}(\tau)^2 \right\rangle_{\mathbf{R}_k}}{2d\tau P(\tau)} = \frac{\sum_{i \in \mathbf{R}_k} [\mathbf{r}_i(\tau) - \mathbf{r}_i(0)]^2}{2d\tau N(0,\tau)} .$$ Eq. 4.3

This equation can be used for the molecules moving parallel to the interface in the two dimensions (x and y in this case, so $d = 2$). The entire time interval used to determine $D_{//}$ is 10 ns. Clearly the 10 nanosecond was too short of a time to estimate the true diffusion coefficient, but longer times would correspond with a lower $N(0,\tau)$, and far fewer particles being included in the calculation of $\langle \Delta \mathbf{r}(t)^2 \rangle_{\mathbf{R}_k}$. There has to be a balance between calculation time, region size (larger regions would obviously allow longer times with reasonable sampling), and desired precision.

The lithium transference number in the xy directions (τ_+^{xy}) can be obtained by Eq. 2.25, since the number of cations and anions are equal, the equation reduces to:

$$\tau_+^{xy} = \frac{N_+ D_+^{xy}}{N_+ D_+^{xy} + N_- D_-^{xy}} = \frac{D_+^{xy}}{D_+^{xy} + D_-^{xy}} .$$ Eq. 4.4

4.2.4.2 Conductivity parallel to an interface

Using the Einstein relation Eq. 2.21, the conductivity parallel to the interface is calculated by substituting $V_{\mathbf{R}_k}$ for V to present the specified region $\mathbf{R}_k$ and $d = 2$ for two dimensions, the equation becomes:

$$\lambda^{xy} = \lim_{t \to \infty} \frac{e^2}{4t V_{\mathbf{R}_k} k_B T} \sum_{i=1}^{N} \sum_{j=1}^{N} z_i z_j \left\langle [\mathbf{r}_i(t) - \mathbf{r}_i(0)] \bullet [\mathbf{r}_j(t) - \mathbf{r}_j(0)] \right\rangle .$$ Eq. 4.5

4.3 Results and Discussion

4.3.1 Density Profiles

The local mass density for species i along the z-direction, $\rho_i(z)$ is in units of g cm^{-3} and can be given by the equation below:

$$\rho_i(z) = \frac{M_i(z)}{N_A V(z)},$$

Eq. 4.6

where $M_i(z)$ is the molecular weight for the species i at postion z, $V(z)$ is the volume at position z, and N_A is Avogadro's number (6.02245×10^{23} molecule mol^{-1}).

To express an approximate trend of each species in the current system, the density in each arbitrary unit was used. Figure 4.3 shows the density profile in arbitrary units of each of the species in SOLID systems at 320 K. Obviously, PEO had a fairly consistent concentration throughout, but showed substantial density oscillations at the surface. Both systems showed significant PEO density oscillations and the largest region of LiClO$_4$ depletion.
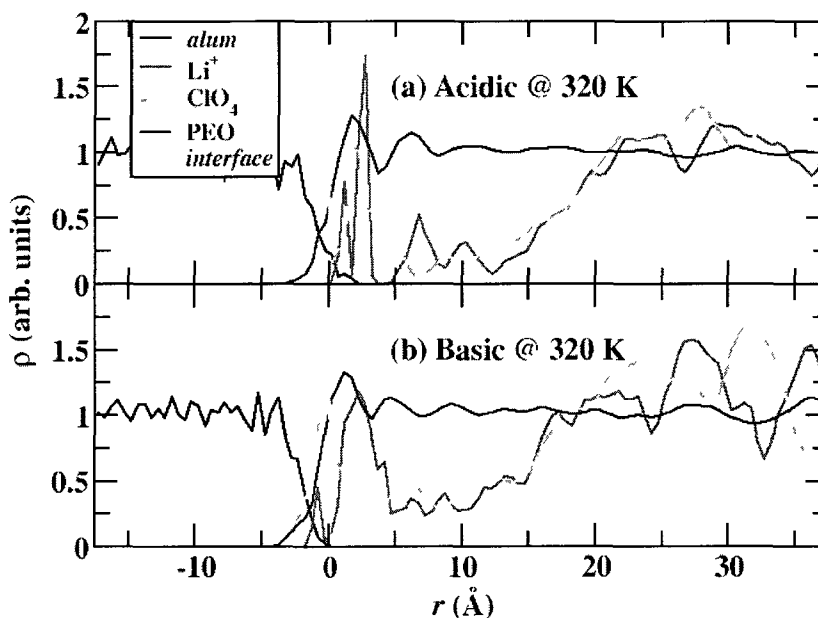
Figure 4.3 Density profiles of each species for SOLID systems investigated at 320 K

A high LiClO$_4$ concentration was near the interface at all temperatures investigated (the other two temperatures are not shown here). Furthermore, the interfacial density of LiClO$_4$ was higher in the ACIDIC system than in the BASIC system in real

density (not shown here). It showed that the ions could bind strongly with alumina, especially with alumina with a hydroxyl terminal group in an acidic system.

4.3.2 Conductivities

One of the goals of this work is to determine the conditions that maximize ionic conductivity and transference for battery operation. For determination of the conductivity λ, Eq. 2.22 without t has to be plotted as a function of t, which should be linear at long enough times, and the slope of this linear region is the ionic conductivity. The conductivities calculated in three dimensions and the xy dimensions for BULK systems studied are listed in Table 4.3, along with sets of experimental data. For the BULK system, the calculation was extended to 460 ns, and 200 ns for SOLID systems. There were many experimental values found in the literature for the conductivity of PEO-LiX with either oxygen to lithium ratios ranging from 8:1 to 23:1, but only two experiments studied, PEO-LiClO$_4$ with EO:Li = 16:1 in 2004 by B.-K. Choi and Y.-W. Kim [157] and with EO:Li = 14:1 in 2010 by S. Fullerton-Shirey and J. Maranas [27], were close to our BULK and SOLID system values. The experimental data shown in Table 4.1 is two times larger than the simulation results at 320 and 348 K. It has been argued that including polarizability in the molecular models will increase the conductivity [123]. For our models, polarizability was not included, which might be the potential explanation for the conductivity being lower than that in the experiment. S. K. Fullerton-Shirey and J. K. Maranas worked with a ratio of EO:Li = 14:1 and no nanoparticles gave that the conductivity shows 0.4×10^{-4} S cm^{-1} at 50 °C (323 K) and a sharp decrease at 40 °C (313 K), where the ionic conductivity is equal to 0.16×10^{-5} S cm^{-1}. The simulation result at 320 K was located between these two experimental results, showing good agreement.

Table 4.3 Comparison of conductivities for bulk simulation results and experiments in 3-dimensions. Along with xy dimension in SOLID systems studied

	Syst.	320 K	348 K	373 K
$\lambda^{3D} \times 10^{-4}$ (S/cm)	Expt.[a]	0.79	3.67	6.61
	BULK	0.37 ± 0.02	1.89 ± 0.46	6.04 ± 1.45
$\lambda^{xy} \times 10^{-4}$ (S/cm)	BULK	0.40 ± 0.03	2.02 ± 0.63	6.51 ± 1.75
	ACIDIC	0.65 ± 0.16	1.56 ± 0.35	1.71 ± 0.73
	BASIC	0.42 ± 0.08	2.10 ± 0.88	8.54 ± 0.41

[a] reference [157] for $(EO)_{16}LiClO_4$.

For the SOLID systems, the conductivities parallel to an interface λ^{xy} show an increase only at 320 K, but no significant increases for the other cases. Experimental work varies significantly due to the effect of alumina [27], but the ACIDIC generally has a higher conductivity than the BASIC, and alumina nanoparticles generally influence at lower temperatures rather than higher. In our work, the biggest effect was at 320 K and with acidic alumina surface system, which ass showing a strong qualitative agreement with S. Fullerton-Shirey and J. Maranas [27]. S. Fullerton-Shirey and J. Maranas worked on PEO – α-Al_2O_3 – $LiClO_4$ systems with a ratio of EO:Li ranging from 14:1 to 8:1 and Al_2O_3 nanoparticle concentrations ranging from 5 to 25 wt%, pointing that the higher conductivity appeared at 10 wt% Al_2O_3. They also indicated that the nanoparticles Al_2O_3 improve conductivity at all temperatures, but the biggest effect is closer to the eutectic point, which is 323 K for an EO:Li ratio of 14:1.

4.3.3 Diffusion and Lithium Transference

Diffusion coefficients parallel to an interface (D^{xy}) were calculated for each of the species, which were straightforward using Eq. 4.3 described in the Section 4.3.2 in the MD simulation. The slope of MSD vs. time was calculated for all systems studied and listed in Table 4.4. It can be observed that for the BULK system, the simulation times

were extended 200-260 ns and were found to have the same slope as the previous 200 ns within the error of calculation. Besides diffusion, a common property calculated to determine the quality of the electrolyte is lithium transference parallel to an interface (τ_+^{xy}) which was calculated using Eq. 4.4 and given along with D^{xy} in Table 4.4. We could not find a value parallel to an interface in experiments for a system using PEO-LiClO$_4$ with or without Al$_2$O$_3$.

Table 4.4 Conductivities, diffusion coefficients of Li$^+$ and ClO$_4^-$, and transference numbers in xy dimensions for 200 ns simulation time for all simulations

	Syst.	320 K	348 K	373 K
$D^{xy}{}_{Li} \times 10^{-8}$ (cm^2/s)	BULK	0.38 ± 0.03	1.26 ± 0.35	2.02 ± 0.22
	ACIDIC	0.75 ± 0.26	1.15 ± 0.04	1.53 ± 0.25
	BASIC	0.54 ± 0.20	1.52 ± 0.00	2.36 ± 0.57
$D^{xy}{}_{ClO4} \times 10^{-8}$ (cm^2/s)	BULK	0.85 ± 0.09	4.09 ± 0.96	10.30 ± 0.28
	ACIDIC	1.26 ± 0.24	3.59 ± 0.17	6.75 ± 1.40
	BASIC	1.00 ± 0.16	5.57 ± 0.62	13.46 ± 2.09
τ_+^{xy}	BULK	0.30 ± 0.01	0.23 ± 0.02	0.14 ± 0.02
	ACIDIC	0.33 ± 0.07	0.24 ± 0.02	0.19 ± 0.06
	BASIC	0.32 ± 0.07	0.22 ± 0.02	0.15 ± 0.01

Apparently, alumina surfaces increase lithium transference at all temperatures, but fairly little increase in a basic surface. With the addition of acidic alumina systems, showing the largest τ_+^{xy} increase due to the largest D_{Li+}^{xy} increase at 320 K, while for other temperatures the τ_+^{xy}s increase was due to the smaller D_{Li+}^{xy} decrease at other temperatures. It could be possible for the -OH group to have more effect on lithium at 320 K.

4.3.4 Conductivities, Diffusion and Lithium Transference in *xy*-directions in Each Region

For determination of the mechanism of ions in individual slabs, λ^{xy}, D_i^{xy}, and τ_+^{xy} were calculated for each ion that stayed in a 10 Å slat for 10 ns (Figure 4.2). Figure 4.4 shows the value of λ^{xy} in each region for SOLID systems at 320 K. Combined with density profiles in Figure 4.3, it shows that the regions in which the value of λ^{xy} was lower, the $LiClO_4$ density was the lowest, except the region close to the interface since the lithium could be bonded strongly to the surface.
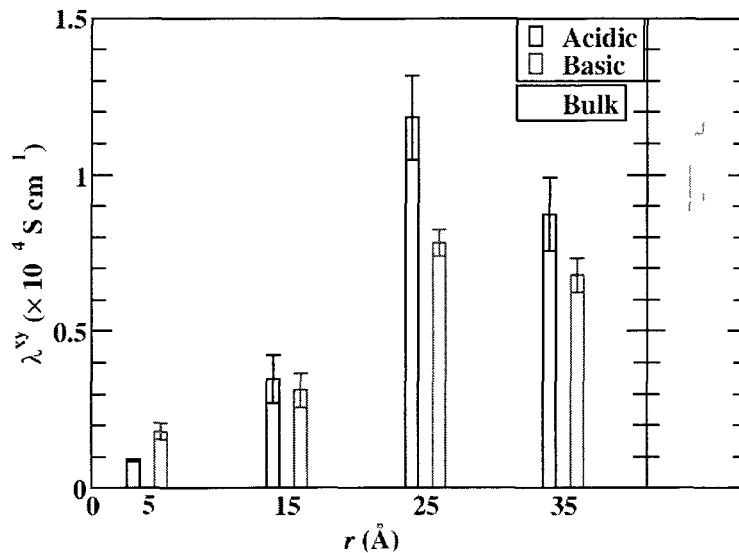
Figure 4.4 λ^{xy} in each region for SOLID systems along with BULK system at 320 K

With the exception of the region close to interface, the λ^{xy}s in other regions was higher for acidic systems than it is for basic systems. Comparing SOLIDs' results with BULK's, it is obvious that the two dimensional conductivities were lower everywhere than for the BULK system. This low result has to do with how the ions bind together. Based on this result, it can be concluded that the lithium is binding more strongly to ClO_4^- in the 0-10 Å region for ACIDIC system at 320 K.

Figure 4.5 and Figure 4.6 give the value of D_i^{xy} where i is Li^+ or ClO_4^-,

respectively, from 10 ns simulation runs. The diffusion was slow close to both solid

interfaces, but higher farther away. Within 10-20 Å away from the solid surface,

diffusion was enhanced for the acidic system in comparison with the basic system,

whereas 20-40 Å away from the solid surface, diffusion was slightly faster for the acidic

system than the basic system. It is of interest that for the region near the interface, when

an -OH group was added to the system, lithium diffusion was the same as the basic

system, but the ClO_4^- diffusion was lower than basic system. It could be possible that

lithium and ClO_4^- have a stronger binding with the solid surface with a hydroxyl group.
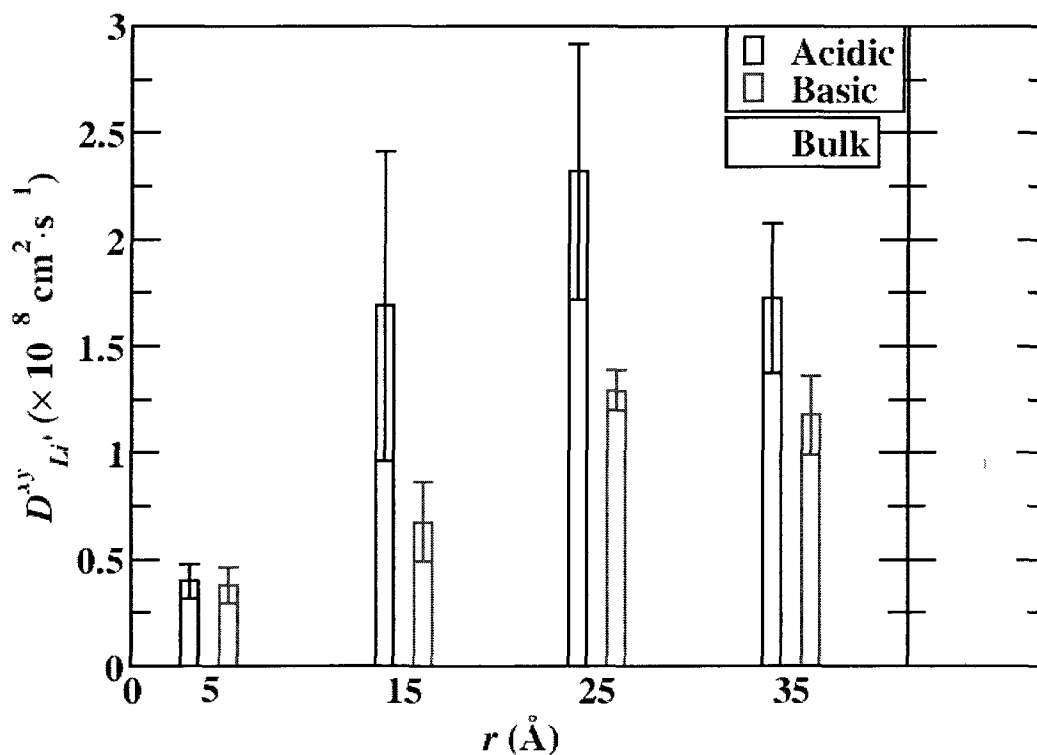
Figure 4.5 $D_{Li^+}^{xy}$ in each region for SOLID systems along with BULK system at 320 K
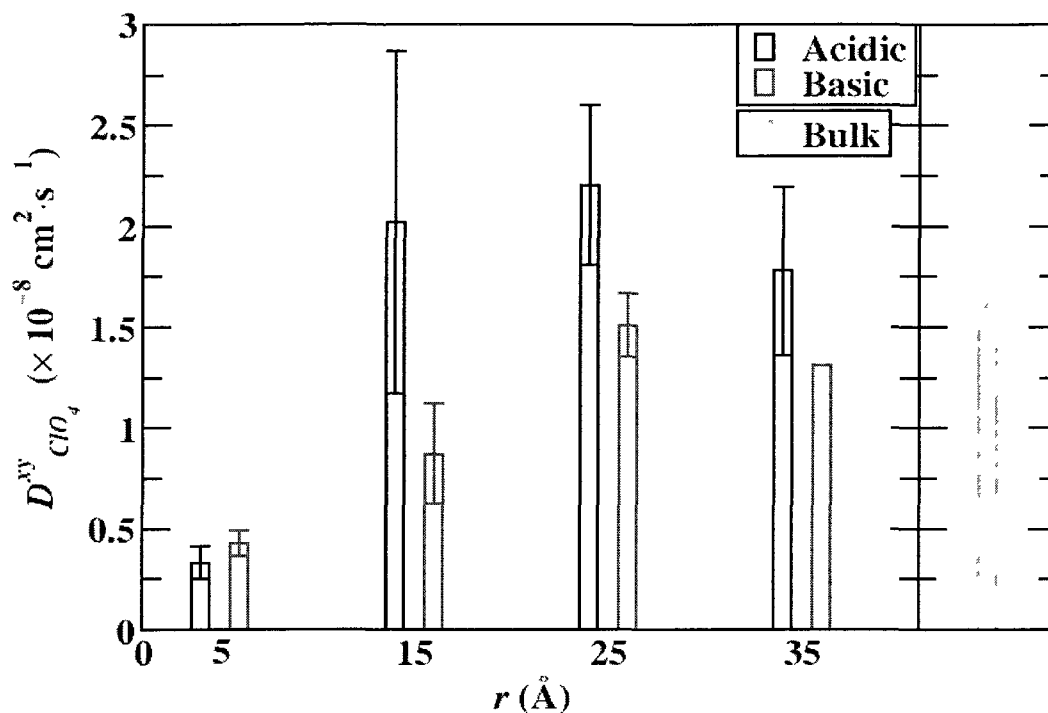
Figure 4.6 $D^{xy}_{ClO_4^-}$ in each region for SOLID systems along with BULK system at 320 K

The lithium transferences (τ_+^{xy}) for each region were calculated from the values of the xy dimensional conductivity of the ions by using Eq. 4.4 and listed in Table 4.5. For comparison, the values of τ_+^{xy} for BULK systems are also shown in the table. Apparently, the addition of the Al_2O_3 surface, especially for the ACIDIC system, had a greater benefit to enhance τ_+^{xy}. The highest increase was shown in the region close to surface for the ACIDIC system at 320 K possibly due to lower $D^{xy}_{ClO_4^-}$. For others, the highest transference was shown in the region farther away from the interface, mostly related to the higher $LiClO_4$ density in these regions (Figure 4.3).

Table 4.5 Lithium transference number (τ_+^{xy}) in each region
for SOLID systems investigated

τ_+^{xy}	(Å)	320 K	348 K	373 K
BULK		0.38 ± 0.02	0.41 ± 0.02	0.32 ± 0.02
ACIDIC	5	0.55 ± 0.03	0.54 ± 0.00	0.50 ± 0.00
	15	0.45 ± 0.01	0.43 ± 0.01	N/A
	25	0.51 ± 0.03	0.56 ± 0.08	0.51 ± 0.07
	35	0.49 ± 0.01	0.51 ± 0.03	0.47 ± 0.02
BASIC	5	0.46 ± 0.02	0.47 ± 0.07	0.50 ± 0.02
	15	0.44 ± 0.01	0.53 ± 0.12	0.35 ± 0.11
	25	0.46 ± 0.03	0.53 ± 0.02	0.61 ± 0.15
	35	0.48 ± 0.05	0.54 ± 0.06	0.52 ± 0.03

4.3.5 Structures

The structure of the system was investigated by calculating the radial distribution functions of lithium with all oxygen atoms with which it had significant binding activity. The RDFs as a function of the z-dimension between lithium and EO oxygen or ClO_4^- oxygen for the SOLID systems along with the BULK system investigated at 320 K are given in Figure 4.7 and Figure 4.8. The RDFs between lithium and alumina oxygen near the interface for SOLID systems studied at all temperatures are shown in Figure 4.9. Lithium did not show any significant binding with any other atoms than the ones shown. The average first lithium EO oxygen RDF peak was centered at a distance of 1.95 Å, 2.00 Å for lithium ClO_4^- oxygen, and 1.85 Å for lithium alumina oxygens for SOLID systems.
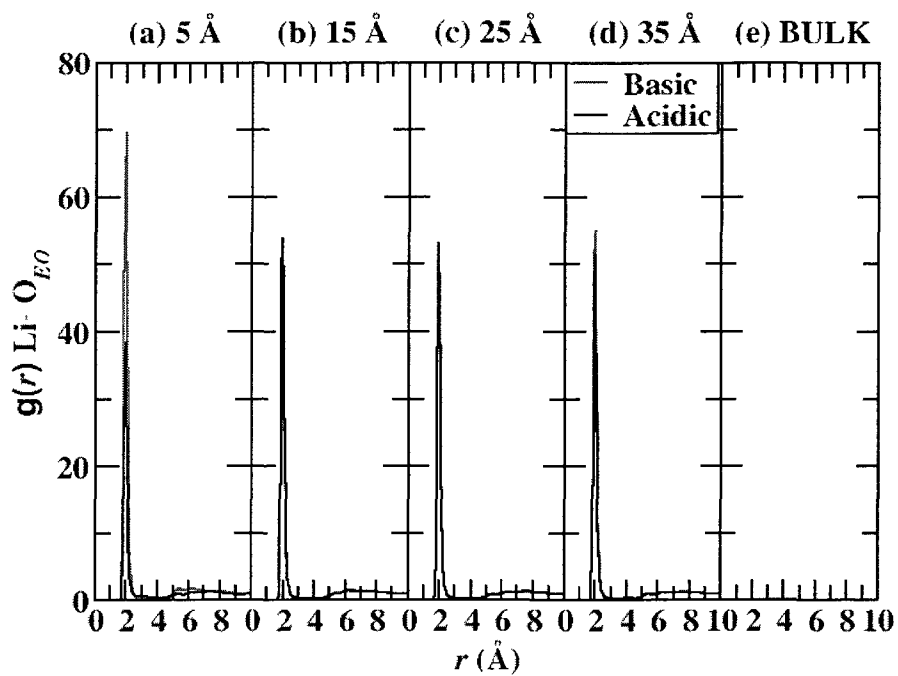
Figure 4.7 RDF at 320 K for lithium with EO oxygens in 5 Å, 15 Å, 25 Å, and 35 Å regions
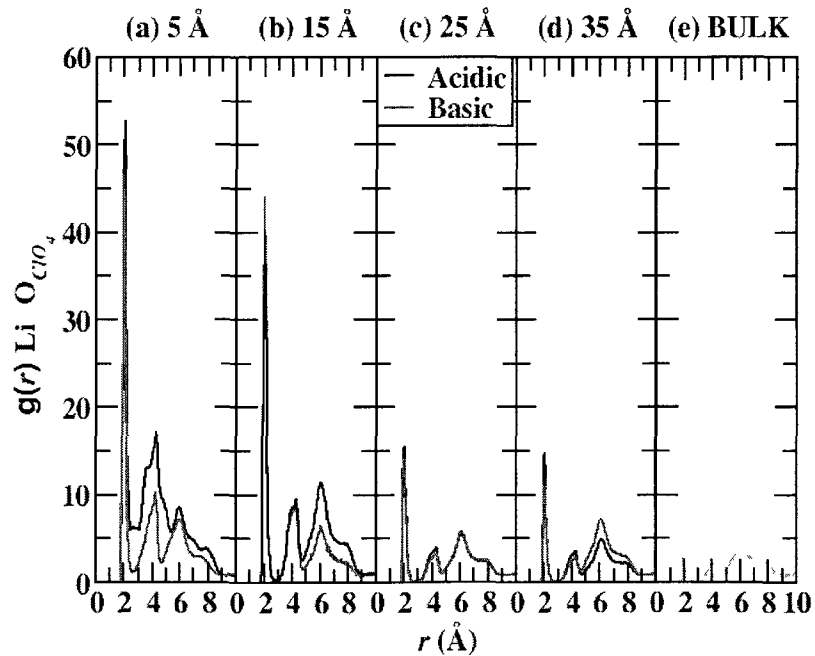
Figure 4.8 RDF at 320 K for lithium with ClO_4^- oxygens in 5 Å, 15 Å, 25 Å, and 35 Å regions
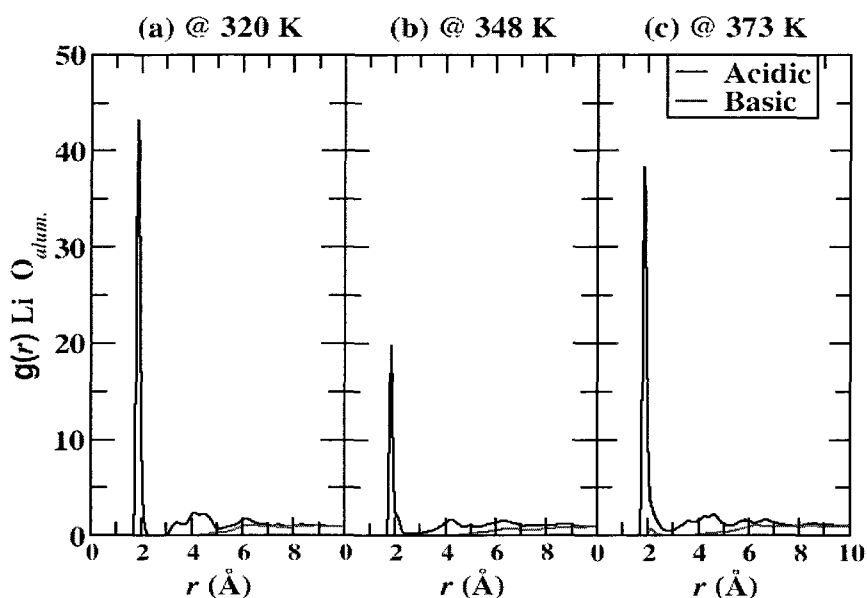
Figure 4.9 RDF for lithium with surface oxygens at (a) 320 K, (b) 348 K, and (c) 373 K investigated

The addition of both basic alumina and acidic alumina increased the strength of lithium binding with ether oxygens and ClO_4^- oxygens. The strength of the lithium coordination is in the following order for BASIC system: Li-O(EO) > Li-O(ClO_4^-) >>> Li-O(alum.) since there was no significant binding between lithium and alumina oxygens at lower temperatures. However, the strength of the lithium binding order was a different story for ACIDIC system, which was Li-O(ClO_4^-) > Li-O(alum.) > Li-O(EO), as evidenced by the RDF peak height. This order brings some insight into why the addition of basic alumina did not have a significant influence on lithium diffusion, as lithium will bind most strongly with EO oxygens. For the addition of alumina with an OH group for the ACIDIC system, the weaker binding ClO_4^- appears to have slightly altered the Li-EO oxygen binding.

With the ACIDIC system, lithium showed a greater degree of binding with the solid oxygens, obviously due to the hydroxide group, showing that oxygens in acidic

alumina may actually induce stronger interactions between lithium and ClO_4^-. Multiple 10 ns blocks of simulations were compared to make sure that this was not due to statistical noise, and in all comparisons with BULK system, the Li-$O(ClO_4^-)$ increased dramatically with the addition of alumina with -OH group, and had a slight effect on the Li-$O(EO)$ RDF.

Figure 4.10 gives the RDFs for ether oxygens with alumina oxygens near interface for SOLID systems investigated at all temperatures. The average first ether oxygen with alumina oxygen peak was located at 2.5 Å for ACIDIC system, showing a significant degree of binding (probably with a lithium ion bridging them) with the acidic surface only. The strength of O(EO)-O(alum.) decreased when the temperature is increased for the ACIDIC system. It showed that there were hydrogen bonds between the surface alumina and PEO oxygens. Even though no significant binding shows in the basic system, there was still structure next to the surface of basic oxygens, but weakly.
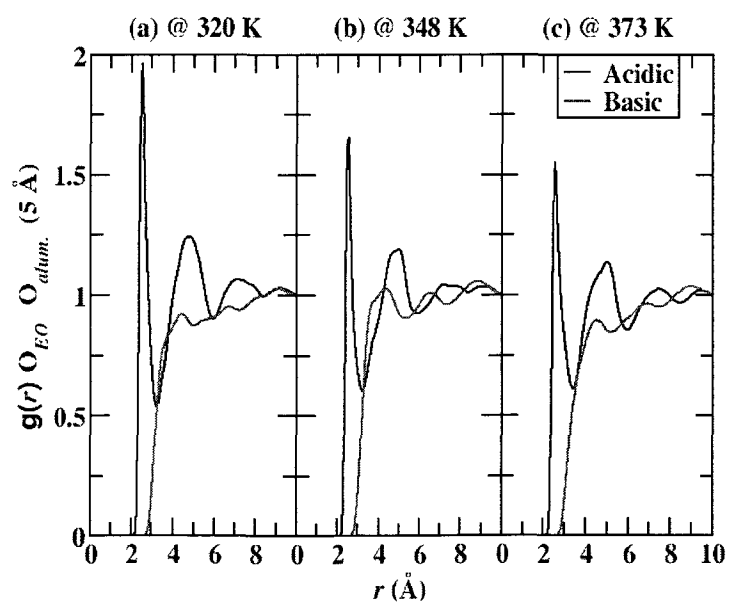
Figure 4.10 RDF for EO oxygens with alumina oxygens for SOLID systems investigated at all temperatures

A snapshot of the interface region taken from the ACIDIC system at 320 K is shown in Figure 4.11. A schematic of the cluster in the middle of the snapshot is illustrated in Figure 4.12. Here, the alumina's surface with hydroxyl terminal groups was expected to favor interactions (via hydrogen bonding) with both the lithium and the PEO segments. This interaction reflects enhancement in the lithium ion transference number in ionic conductivity. These are the origins of the higher first peak shown in the RDF of O(EO)-O(alum.), and Li-O(alum.) for ACIDIC system. The hydroxyl group appeared to have a small effect on the ability of the system to form clusters of these types.
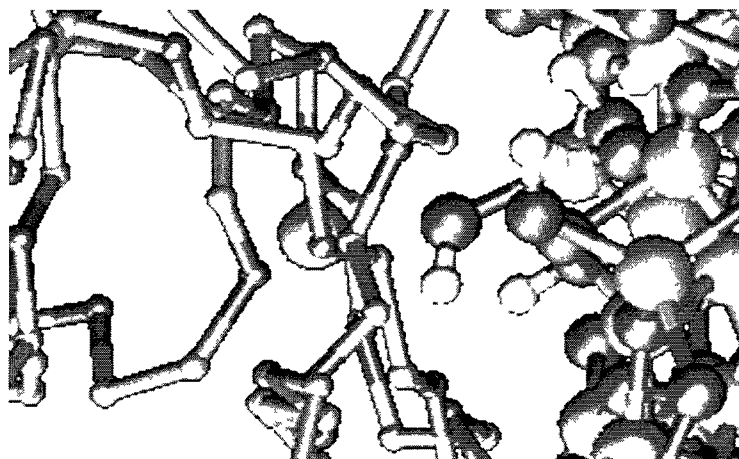
Figure 4.11 A snapshot of a cluster of molecules taken from the ACIDIC system at 320 K, in which, green is Li, yellow is Cl, grey indicates Al, white is H, and red is O
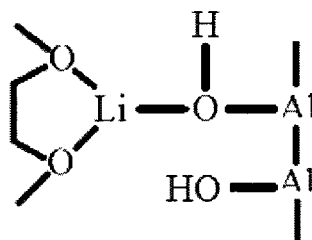
Figure 4.12 A schematic of a representative cluster shown in Figure 4.11

These cluster molecules shown are similar as in Croce et al. 2001,[73] and may involve specific interactions between the alumina and both PEO segments and the lithium salt anions, which may be further interpreted in terms of Brønsted or Lewis acid-base interactions [16]. Brønsted-type acid centers are formed by an -OH group on the surface. Ether oxygen of PEO is a Lewis base; the lithium cation is rather a strong Lewis acid, and the ClO_4^- anion is a Lewis base, there is a probability of diverse reactions of an acid-base nature in these composite systems. The final ultrastructure and later the mechanism of the systems under study was a result of equilibrium between various Lewis acid-base reactions.

4.3.6 Lithium Residence Times

There are generally three mechanisms that will be considered for lithium movement in PEO-LiClO$_4$ for SOLID systems. One is the movement of lithium hopping from one oxygen molecule to the other, and the others are movement in a vehicular mechanism while lithium is bonded with either a ClO_4^- or alumina oxygen, or both species. For a better understanding of how the inclusion of alumina influence these mechanisms, the residence times were calculated for lithium with each oxygen with which it was found to bind strongly. Here, Eq. 3.2, an ACF, was used. Lithium was considered to be coordinated with oxygen when their distance was less than 2.5 Å, near the minimums after the first Li-O RDF peaks. The ACF as a function of time is given in Figure 4.13 on a logarithmic scale. For the ACIDIC system, it is clear that binding with the alumina oxygen lasted much longer than binding with ClO_4^- and EO oxygen. In contrast, lithium binding with basic alumina oxygen to a similar degree as with ClO_4^-, having its ACF falling off much faster than with EO oxygen.
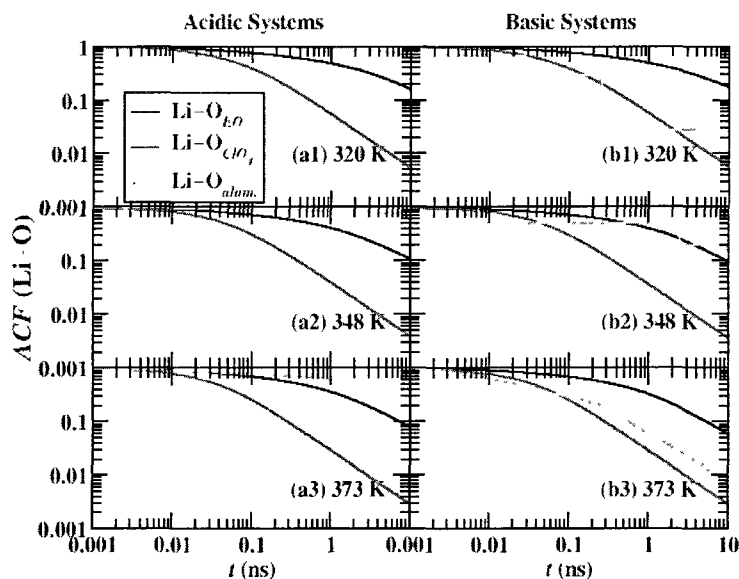
Figure 4.13 Residence time ACFs of lithium moving along PEO, ClO_4^-, and alumina surfaces for all simulations

The mean residence times themselves, τ_{res}, were calculated by fitting ACFs to $\exp[-(x/\tau_{res})^\beta]$, where β and τ_{res} were fit. The value of β ranged from 0.3 to 0.8. The results for τ_{res} are listed in Table 4.6. For all cases in the ACIDIC system, the shortest τ_{res} was for lithium binding with ClO_4^-, and the longest τ_{res} was with the alumina oxygen. However, for all cases in the BASIC systems, the shortest τ_{res} was for lithium binding with alumina oxygen, and the longest τ_{res} was with ether oxygen. The values of τ_{res} binding with EO and ClO_4^- increased at lower temperatures and decreased when the temperature increased. It is of interest that for both systems, the longest τ_{res} for lithium binding with alumina oxygen were at 348 K. Apparently, the species lithium most strongly binds with alumina oxygen for ACIDIC systems and with EO oxygen for BASIC systems, evident in RDFs. Overcoming the binding of Li-O(EO) for BASIC systems is what mostly promotes lithium mobility.

Table 4.6 Mean Residence time (τ_{res}) for lithium binding with EO oxygens, ClO_4^-, and alumina oxygens for all SOLID systems studies at all temperatures

	τ_{res}(ns)	320 K	348 K	373 K
ACIDIC	Li-O$_{EO}$	2.11 ± 0.06	1.29 ± 0.03	0.93 ± 0.03
	Li-O$_{ClO4}$	0.12 ± 0.01	0.08 ± 0.00	0.06 ± 0.00
	Li-O$_{alum}$	51.56± 6.20	188.89 ± 90.33	20.19 ± 9.79
BASIC	Li-O$_{EO}$	2.30 ± 0.05	1.20 ± 0.06	0.77 ± 0.01
	Li-O$_{ClO4}$	0.11 ± 0.01	0.08 ± 0.00	0.06 ± 0.00
	Li-O$_{alum}$	0.05 ± 0.00	1.64 ± 0.00	0.05 ± 0.02

The ACFs for lithium binding with each oxygen in special regions were also calculated for SOLID systems (not shown here). The τ_{res}s were calculated by fitting ACFs to the same equation shown above, and the results for τ_{res}s are given in Figure 4.14 and Figure 4.15. For lithium binding with ether oxygen, the residence time was decreased when temperature increased for all regions except one, the 5 Å where τ_{res} was the highest at 348 K for ACIDIC. The longest τ_{res} was in the region 5 Å from the interface for both SOLID systems at 320 K, showing that the binding between lithium and EO oxygen was strong at lower temperature when lithium moved close to interface. For lithium binding with ClO_4^- oxygen, the relationship was similar to that of lithium and ether oxygen; the alumina surface increased the residence time at 320 K and decreased residence time at 373 K. Apparently, the species that lithium most strongly binds with are EO oxygens, and overcoming this binding is what promotes lithium mobility.
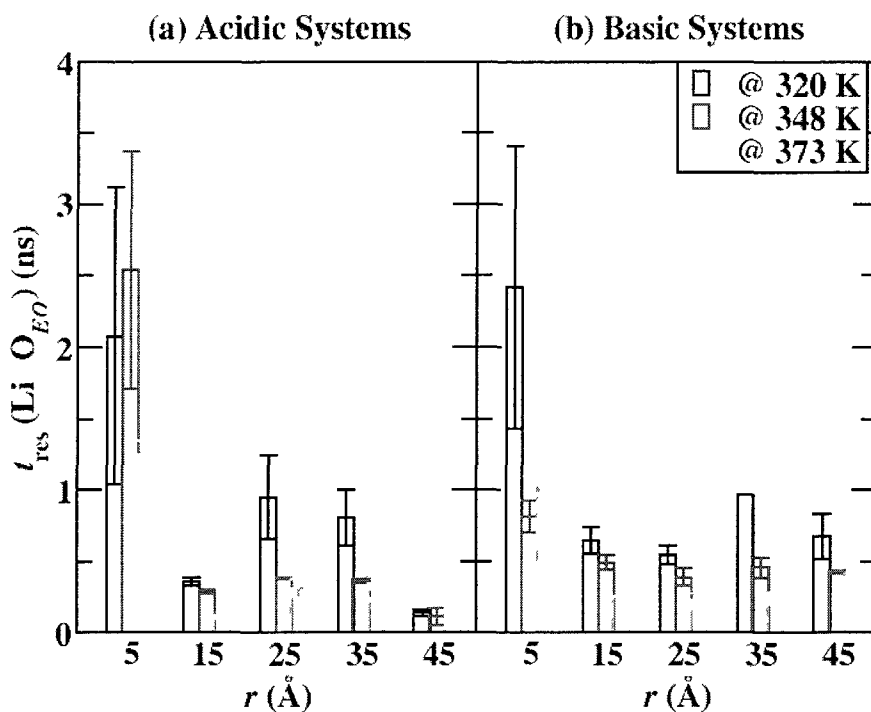
Figure 4.14 Residence time of lithium moving along PEO for all simulations
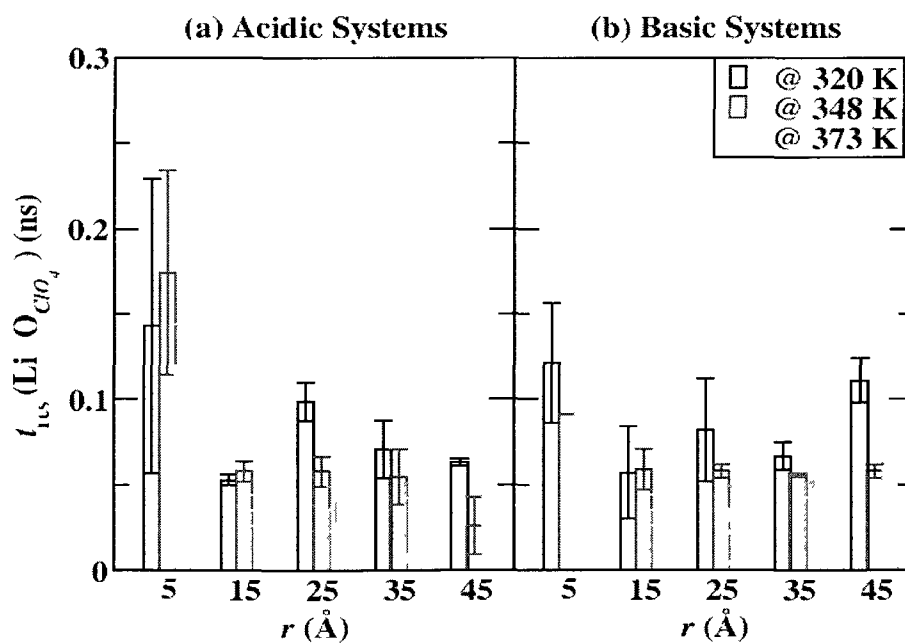
Figure 4.15 Residence time for ACFs of lithium moving along ClO_4^- for all simulations

4.4 Conclusions

Molecular dynamics simulations, aided by Monte Carlo simulations for equilibration, were used to understand how the addition of an alumina surface influences ionic conduction and lithium transference for solid polymer electrolytes of LiClO$_4$ in poly(ethylene oxide) with a number-averaged molecular weight of 10,000 g/mol. The acidic surface showed the strongest binding with ions, essentially freezing their movement at the surface, but a modest enhancement in lithium ion mobility was observed at 320 K. In general, the surface had little effect on overall ionic mobility, reducing it near the surface, while showing slight enhancement a 20 Å away from it.

CHAPTER 5

FINAL CONCLUSIONS AND FUTURE WORK

5.1   Final Conclusions

A combination of molecular dynamics and Monte Carlo simulations were used to bring insight into lithium ion transport in poly(ethylene oxide) (PEO) with lithium salts added with plasticizers and next to alumina solid surface doped with lithium salt. Current methods are not adequate to enhance lithium ion mobility in PEO to make polymer electrolytes viable for usage in rechargeable lithium ion batteries. The results showed that while ionic conductivity increased to a moderate degree with the addition of plasticizers, the lithium diffusion itself showed very little change. The enhancement in ionic conductivity was primarily due to increased anion diffusion. The presence of the alumina surface had little effect on lithium ion mobility in PEO with lithium salts. However, at the lowest temperatures simulated, 320 K, an alumina surface treated with acid so that many of its oxygens were hydroxylated, small increases in ionic conductivity and lithium ion transport were observed. This increase had less to do with interactions between lithium and the alumina surface itself, as lithium ions near the surface had little mobility, but was due to faster transfer 1-2 nm away from the lithium surface. The work carried out to investigate lithium ion mobility in PEO shows that many of the current strategies to enhance lithium ion mobility in these polymer electrolytes are not adequate

to bring lithium ion mobility nearly high enough for viable usage and new strategies are required.

5.2   Future Work

Our work showed that plasticizers and solid surfaces only had marginal influences on lithium ion mobility. However, adding these two together may have a greater influence. In addition, we can try other plasticizers. My previous research found that alumina surfaces can show potential enhancements in lithium ion mobility, but cyclic plasticizers do not show much of an effect. If further plasticizers can be investigated, and some are found to promote small to moderate enhancements in lithium ion mobility, they can be placed next to a surface to see if further enhancement is possible. This strategy of combining multiple avenues for enhanced lithium ion mobility may be enough to bring it high enough to make polymer electrolytes viable for rechargeable lithium batteries.

APPENDIX A

SOURCE CODE FOR CONDUCTIVITY

```
SUBROUTINE conductivity

call diffusion                          see Appendix B
cnd=0.0d0
do i=1,nres                             calculate double summation part in
                                        Eq. 2.21. Only ions have charge, +1
                                        or -1, other molecules are neutrals in
                                        this work.

   do j=1,nres
      if (i.le.j) then
         do m=1,3                       in three dimensions
            cnd=cnd+chrg(i)*chrg(j)*com(m,i)*com(m,j)
         end do
      end if
   end do
end do
dim=3.0
vol=box(1)*box(2)*box(3)
const=ele**2.0/(2.0*dim*vol*kb*temp0)
cnd=cnd*const*1.0d20                     change unit to S/cm
return
end subroutine
```

APPENDIX B

SOURCE CODE FOR DIFFUSION COEFFICIENT

```
SUBROUTINE diffusion

if (iinit.eq.1) then                        initialize some values
   do i=1,natom
      do m=1,3
         xo(m,i)=xi(m,i)                     save old position
         xid(m,i)=0.0d0
      end do
   end do
else if (iinit.eq.2) then                   begin to calculate MSD
   do i=1,natom
      do m=1,3
         xio(m)=xi(m,i)-xo(m,i)             calculate the distance move within
                                            time t to t+dt

         call pbc                            Periodic Boundary Condition
         xid(m,i)=xid(m,i)+xio(m)
         xo(m,i)=xi(m,i)                     save old position
      end do
   end do

   do it=1,ntype                            initialize some values
      msd(it)=0.0d0
      count(it)=0
   end do
   do ii=1,nres
      do m=1,3
         com(m,ii)=0.0d0
      end do
   end do
   do ii=1,nres
      it=itype(ipres(ii))
      tamass=0.0d0
      count(it)=count(it) + 1               count the number of each molecule
      do i=ipres(ii),ipres(ii+1)-1          calculate center-of-mass for every
                                            molecule
         tamass=tamass+amass(i)
         do m=1,3
            com(m,ii)=com(m,ii)+
               amass(i)*xid(m,i)
         end do
      end do
      do m=1,3                              calculate MSD for each molecule in
                                            three dimensions
         com(m,ii)=com(m,ii)/tamass
         msd(it)=msd(it)+com(m,ii)**2
      end do
```

```
      end do
      do it=1,ntype
          msd(it)=msd(it)/dble(count(it))
      end do
   end if
   return
   end subroutine
```

APPENDIX C

SOURCE CODE FOR RADIAL DISTRIBUTION FUNCTION

```
SUBROUTINE rdf

if (iinit.eq.1) then                        initialize some values
    do it=1,ntype
        npart(it)=0
        do jt=1,ntype
            do bin=1,maxbin
                hist(bin,it,jt)=0.0d0
                nhist(bin,it,jt)=0
            end do
        end do
    end do
    do i=1,natom                             calculate number of each type of
                                             atoms

        it=itype(i)
        npart(it)=npart(it)+1
    enddo
    dr=rcut/dble(maxbin)
    vol=box(1)*box(2)*box(3)
else if (iinit.eq.2) then
    do i=1,natom-1
        it=itype(i)
        do j=i,natom
            jt=itype(j)
            rij=0.0d0
            do m=1,3                         calculate distance between atom i
                                             and j
                xij(m)=xi(m,i)-xi(m,j)
                call pbc
                rij=rij+xij(m)**2
            end do
            rij=dsqrt(rij)
            bin=int(rij/dr)+1
            if (bin.le.maxbin) then
                if (it.le.jt) then
                    hist(bin,it,jt)=hist(bin,it,jt)+1.0d0
                    nhist(bin,it,jt)=nhist(bin,it,jt)+1
                else
                    hist(bin,jt,it)=hist(bin,jt,it)+1.0d0
                    nhist(bin,jt,it)=nhist(bin,jt,it)+1
                end if
            end if
        end do
    end do
else                                         normalize RDF
    do bin=1,maxbin
        r=dr*dble(bin)
```

```
      vb=r**3.0-(r-dr)**3.0
      do it=1,ntype
          do jt=1,ntype
              rho=dble(npart(jt))/vol
              nideal=(4.0/3.0)*pi*vb*rho
              hist(bin,it,jt)=hist(bin,it,jt)/dble(npart(it))
                              /dble(nhist(bin,it,jt))/nideal
          end do
      end do
   end do
end if
return
end subroutine
```

APPENDIX D

SOURCE CODE FOR COORDINATION NUMBER

```
SUBROUTINE CordNum

call rdf                                    see Appendix C
cn=0.0d0
do bin=1,maxbin
   r=dr*dble(bin)
   vb=r**3.0-(r-dr)**3.0
   if (r.le.rmin) then                      calculate the number of it atoms in
                                            the jt's first coordination shell
      cn=cn+hist(bin,it,jt)*(4.0/3.0)
         *pi*vb*dble(npart(it))/vol
   end if
end do
return
end subroutine
```

REFERENCES

[1]   T. J. Pinnavaia and G. W. Beall, Polymer-clay nanocomposites. New York: Wiley, 2002.

[2]   F. Croce, *et al.*, "Nanocomposite polymer electrolytes for lithium batteries," *Nature,* vol. 394, pp. 456-458, 1998.

[3]   B. Scrosati, Applications of electroactive polymers: Springer, 1993.

[4]   J. R. MacCallum and C. A. Vincent, *Polymer electrolyte reviews,* vol. 1. London: Elsevier, 1987.

[5]   J. R. MacCallum and C. A. Vincent, *Polymer electrolyte reviews,* vol. 2. London, UK: Elsevier, 1989.

[6]   J. M. Tarascon and M. Armand, "Issues and challenges facing rechargeable lithium batteries," *Nature,* vol. 414, pp. 359-367, 2001.

[7]   K. M. Abraham, "Directions in secondary lithium battery research and development, " *Electrochimica Acta,* vol. 38, pp. 1233-1248, 1993.

[8]   A. Attewell, "The behaviour of lithium batteries in a fire," *Journal of Power Sources,* vol. 26, pp. 195-200, 1989.

[9]   P. G. Balakrishnan, *et al.*, "Safety mechanisms in lithium-ion batteries," *Journal of Power Sources,* vol. 155, pp. 401-414, 2006.

[10]   M. Holzapfel, *et al.*, "Oxygen, hydrogen, ethylene and CO_2 development in lithium-ion batteries," *Journal of Power Sources,* vol. 174, pp. 1156-1160, 2007.

[11]   R. Spotnitz and J. Franklin, "Abuse behavior of high-power, lithium-ion cells," *Journal of Power Sources,* vol. 113, pp. 81-100, 2003.

[12]   F. M. Gray, *Solid polymer electrolytes: Fundamentals and technological applications.* Cambridge, UK: Wiley-VCH Press, 1991.

[13]   F. M. Gray, *Polymer electrolytes.* (Great Britain): Royal Society of Chemistry, 1997.

[14]   I. E. Kelly, *et al.*, "Poly(ethylene oxide) electrolytes for operation at near room temperature," *Journal of Power Sources,* vol. 14, pp. 13-21, 1985.

[15]   J. Xi, et al., "Electrochemistry study on PEO-LiClO$_4$-ZSM5 composite polymer electrolyte," Chinese Science Bulletin, vol. 49, pp. 785-789, 2004.

[16]   W. Wieczorek, et al., "Composite polyether based solid electrolytes. The Lewis acid-base approach," Solid State Ionics, vol. 85, pp. 67-72, 1996.

[17]   W. Wieczorek, et al., "Ionic interactions in polymeric electrolytes based on low molecular weight poly(ethylene glycol)s," The Journal of Physical Chemistry B, vol. 102, pp. 6968-6974, 1998.

[18]   J. E. Weston and B. C. H. Steele, "Effects of preparation method on properties of lithium salt-poly(ethylene oxide) polymer electrolytes," Solid State Ionics, vol. 7, pp. 81-88, 1982.

[19]   J. E. Weston and B. C. H. Steele, "Effects of inert fillers on the mechanical and electrochemical properties of lithium salt-poly(ethylene oxide) polymer electrolytes," Solid State Ionics, vol. 7, pp. 75-79, 1982.

[20]   E. Tsuchida, et al., "Lithium ionic conduction in poly (methacrylic acid)-poly (ethylene oxide) complex containing lithium perchlorate," Solid State Ionics, vol. 11, pp. 227-233, 1983.

[21]   C. C. Tambelli, et al., "Characterisation of PEO-Al$_2$O$_3$ composite polymer electrolytes," Electrochimica Acta, vol. 47, pp. 1677-1682, 2002.

[22]   D. Shanmukaraj, et al., "Ionic conductivity and electrochemical stability of poly(methylmethacrylate)-poly(ethylene oxide) blend-ceramic fillers composites," Journal of Physics and Chemistry of Solids, vol. 69, pp. 243-248, 2008.

[23]   B. Scrosati, et al., "Impedance spectroscopy study of PEO-based nanocomposite polymer electrolytes," Journal of The Electrochemical Society, vol. 147, pp. 1718-1721, 2000.

[24]   X. Qian, et al., "Impedance study of (PEO)$_{10}$LiClO$_4$-Al$_2$O$_3$ composite polymer electrolyte with blocking electrodes," Electrochimica Acta, vol. 46, pp. 1829-1836, 2001.

[25]   J. W. Park, et al., "Effect of organic acids and nano-sized ceramic doping on PEO-based solid polymer electrolytes," Journal of Power Sources, vol. 160, p. 674, 2006.

[26]   M. Marcinek, et al., "Effect of filler surface group on ionic interactions in PEG-LiClO$_4$-Al$_2$O$_3$ composite polyether electrolytes," The Journal of Physical Chemistry B, vol. 104, pp. 11088-11093, 2000.

[27]   S. K. Fullerton-Shirey and J. K. Maranas, "Structure and mobility of PEO/LiClO$_4$ solid polymer electrolytes filled with Al$_2$O$_3$ nanoparticles," The Journal of Physical Chemistry C, vol. 114, pp. 9196-9206, 2010.

[28]   C. Capiglia, *et al.*, "Effects of nanoscale SiO_2 on the thermal and transport properties of solvent-free, poly(ethylene oxide) (PEO)-based polymer electrolytes," *Solid State Ionics,* vol. 118, pp. 73-79, 1999.

[29]   T. J. Singh and S. V. Bhat, "Increased lithium-ion conductivity in $(PEG)_{46}LiClO_4$ solid polymer electrolyte with δ-Al_2O_3 nanoparticles," *Journal of Power Sources,* vol. 129, pp. 280-287, 2004.

[30]   J.-W. Choi, *et al.*, "Poly(ethylene oxide)-based polymer electrolyte incorporating room-temperature ionic liquid for lithium batteries," *Solid State Ionics,* vol. 178, pp. 1235-1241, 2007.

[31]   E. H. Cha, *et al.*, "Ionic conductivity studies of polymeric electrolytes containing lithium salt with plasticizer," *Electrochimica Acta,* vol. 50, pp. 335-338, 2004.

[32]   G. Mao, *et al.*, "α-relaxation in PEO-LiTFSI polymer electrolytes," *Macromolecules,* vol. 35, pp. 415-419, 2002.

[33]   E. Zygadlo-Monikowska, *et al.*, "Lithium ion transport of solid electrolytes based on PEO/CF_3SO_3Li and aluminum carboxylate," *Journal of Power Sources,* vol. 173, pp. 734-742, 2007.

[34]   C. Wang, *et al.*, "Investigation on the structure and the conductivity of plasticized polymer electrolytes," *Solid State Ionics,* vol. 53-56, pp. 1106-1110, 1992.

[35]   T. K.-J. Köster and L. v. Wüllen, "Cation-anion coordination, ion mobility and the effect of Al_2O_3 addition in PEO based polymer electrolytes," *Solid State Ionics,* vol. 181, pp. 489-495, 2010.

[36]   I. Kelly, *et al.*, "Mixed polyether lithium-ion conductors," *Journal of Electroanalytical Chemistry and Interfacial Electrochemistry,* vol. 168, pp. 467-478, 1984.

[37]   P. Johansson, *et al.*, "The influence of inert oxide fillers on poly(ethylene oxide) and amorphous poly(ethylene oxide) based polymer electrolytes," *The Journal of Physical Chemistry B,* vol. 105, pp. 9016-9021, 2001.

[38]   L. R. A. K. Bandara, *et al.*, "Ionic conductivity of plasticized(PEO)-$LiCF_3SO_3$ electrolytes," *Electrochimica Acta,* vol. 43, pp. 1447-1451, 1998.

[39]   S. Chintapalli and R. Frech, "Effect of plasticizers on high molecular weight PEO-$LiCF_3SO_3$ complexes," *Solid State Ionics,* vol. 86-88, pp. 341-346, 1996.

[40]   D. Golodnitsky and G. A. a. E. Peled, "Ion-transport phenomena in concentrated PEO-based composite polymer electrolytes," *Solid State Ionics,* vol. 147, pp. 141-155, 2002.

[41]   D. Golodnitsky, *et al.*, "Conduction mechanisms in concentrated LiI-polyethylene oxide-Al_2O_3-based solid electrolytes," *Journal of The Electrochemical Society,* vol. 144, pp. 3484-3491, 1997.

[42]   S. Zhang, *et al.*, "Li^+ conducting 'fuzzy' poly(ethylene oxide)-SiO_2 polymer composite electrolytes," *Journal of Power Sources,* vol. 134, pp. 95-102, 2004.

[43]   B. Kumar and L. G. Scanlon, "Composite electrolytes for lithium rechargeable batteries," *Journal of Electroceramics,* vol. 5, pp. 127-139, 2000.

[44]   J. B. Kerr, "Polymer electrolytes: An overview," in *Lithium batteries: science and technology,* G. Nazri and G. Pistoia, Eds., ed Boston: Kluwer Academic Publishers, 2004, p. 708.

[45]   C. Berthier, *et al.*, "Microscopic investigation of ionic conductivity in alkali metal salts-poly(ethylene oxide) adducts," *Solid State Ionics,* vol. 11, pp. 91-95, 1983.

[46]   Y.-T. Kim and E. S. Smotkin, "The effect of plasticizers on transport and electrochemical properties of PEO-based electrolytes for lithium rechargeable batteries," *Solid State Ionics,* vol. 149, pp. 29-37, 2002.

[47]   S. Lascaud, *et al.*, "Phase diagrams and conductivity behavior of poly(ethylene oxide)-molten salt rubbery electrolytes," *Macromolecules,* vol. 27, pp. 7469-7477, 1994.

[48]   F. M. Gray, *et al.*, "Poly(ethylene oxide)-$LiCF_3SO_3$-polystyrene electrolyte systems," *Solid State Ionics,* vol. 18-19, Part.1, pp. 282-286, 1986.

[49]   W. Gorecki, *et al.*, "NMR and conductivity study of polymer electrolytes in the imide family: $P(EO)/Li[N(SO_2C_nF_{2n+1})(SO_2C_mF_{2m+1})]$," *ChemPhysChem,* vol. 3, pp. 620-625, 2002.

[50]   M. Watanabe, *et al.*, "Ion conduction mechanism in network polymers from poly(ethylene oxide) and poly(propylene oxide) containing lithium perchlorate," *Solid State Ionics,* vol. 18-19, Part. 1, pp. 338-342, 1986.

[51]   R. Strümpler and J. Glatz-Reichenbach, "Conducting polymer composites," *Journal of Electroceramics,* vol. 3, pp. 329-346, 1999.

[52]   X.-G. Sun, *et al.*, "New gel polyelectrolytes for rechargeable lithium batteries," *Solid State Ionics,* vol. 175, pp. 713-716, 2004.

[53]   M. Z. A. Munshi and B. B. Owens, "Performance of polymer electrolyte cells at +25 to +100°C," *Solid State Ionics,* vol. 26, pp. 41-46, 1988.

[54]   G. G. Cameron, *et al.*, "Conductivity and viscosity of liquid polymer electrolytes plasticized by propylene carbonate and tetrahydrofuran," *European Polymer Journal,* vol. 26, pp. 1097-1101, 1990.

[55] R. Huq, *et al.*, "Influence of plasticizers on the electrochemical and chemical stability of a Li$^+$ polymer electrolyte," *Solid State Ionics,* vol. 57, pp. 277-283, 1992.

[56] R. J. Klein and J. Runt, "Plasticized single-ion polymer conductors: conductivity, local and segmental dynamics, and interaction parameters," *The Journal of Physical Chemistry B,* vol. 111, pp. 13188-13193, 2007.

[57] K. M. Abraham, *et al.*, "Highly conductive PEO-like polymer electrolytes," *Chemistry of Materials,* vol. 9, pp. 1978-1988, 1997.

[58] J. J. Xu and H. Ye, "Polymer gel electrolytes based on oligomeric polyether/cross-linked PMMA blends prepared via in situ polymerization," *Electrochemistry Communications,* vol. 7, pp. 829-835, 2005.

[59] L. M. Bronstein, *et al.*, "Solid polymer single-ion conductors: synthesis and properties," *Chemistry of Materials,* vol. 18, pp. 708-715, 2006.

[60] I. Honma, *et al.*, "Synthesis of organic/inorganic nanocomposites protonic conducting membrane through sol-gel processes," *Solid State Ionics,* vol. 118, pp. 29-36, 1999.

[61] Y. X. Li, *et al.*, "Crosslinkable fumed silica-based nanocomposite electrolytes for rechargeable lithium batteries," *Journal of Power Sources,* vol. 161, pp. 1288-1296, Oct 2006.

[62] J. Ennari, *et al.*, "Molecular dynamics simulation of the structure of an ion-conducting PEO-based solid polymer electrolyte," *Polymer,* vol. 43, pp. 5427-5438, 2002.

[63] B.-K. Choi, *et al.*, "Effects of ceramic fillers on the electrical properties of (PEO)$_{16}$LiClO$_4$ electrolytes," *Journal of Power Sources,* vol. 68, pp. 357-360, 1997.

[64] B.-K. Choi and K.-H. Shin, "Effects of SiC fillers on the electrical and mechanical properties of (PEO)$_{16}$LiClO$_4$ electrolytes," *Solid State Ionics,* vol. 86-88, pp. 303-306, 1996.

[65] A. Dey, *et al.*, "Molecular interaction and ionic conductivity of polyethylene oxide-LiClO$_4$ nanocomposites," *Journal of Physics and Chemistry of Solids,* vol. 71, pp. 329-335, 2010.

[66] F. Capuano, *et al.*, "Composite polymer electrolytes," *Journal of the Electrochemical Society,* vol. 138, pp. 1918-1922, 1991.

[67] J. H. Ahn, *et al.*, "Nanoparticle-dispersed PEO polymer electrolytes for Li batteries," *Journal of Power Sources,* vol. 119-121, pp. 422-426, 2003.

[68] F. Croce, *et al.*, "Physical and chemical properties of nanocomposite polymer electrolytes," *The Journal of Physical Chemistry B*, vol. 103, pp. 10632-10638, 1999.

[69] P. A. R. D. Jayathilaka, *et al.*, "Effect of nano-porous Al_2O_3 on thermal, dielectric and transport properties of the $(PEO)_9LiTFSI$ polymer electrolyte system," *Electrochimica Acta*, vol. 47, pp. 3257-3268, 2002.

[70] A. S. Best, *et al.*, "Microscopic interactions in nanocomposite electrolytes," *Macromolecules*, vol. 34, pp. 4549-4555, 2001.

[71] J.-H. Shin, *et al.*, "Comparison of solvent-cast and hot-pressed $P(EO)_{20}LiN(SO_2CF_2CF_3)_2$ polymer electrolytes containing nanosized SiO_2," *Journal of The Electrochemical Society*, vol. 152, pp. A283-A288, 2005.

[72] Z. Florjanczyk, *et al.*, "Review of PEO based composite polymer electrolytes," *Polish Journal of chemistry*, vol. 78, pp. 1279-1304, 2004.

[73] F. Croce, Persi, L., Scrosati, B., Serraino-Fiory, F., Plichta, E., Hendrickson, M. A., "Role of the ceramic fillers in enhancing the transport properties of composite polymer electrolytes," *Electrochimica Acta*, vol. 46, pp. 2457-2461, 2001.

[74] Z. Gadjourova, *et al.*, "Ionic conductivity in crystalline polymer electrolytes," *Nature*, vol. 412, pp. 520-523, Aug 2 2001.

[75] Y. Tominaga, *et al.*, "Ion-conductive properties of mesoporous silica-filled composite polymer electrolytes," *Electrochimica Acta* vol. 50, pp. 3949-3954, 2005.

[76] P. P. Chu, *et al.*, "Novel composite polymer electrolyte comprising mesoporous structured SiO_2 and PEO/Li," *Solid State Ionics* vol. 156, pp. 141-153, 2003.

[77] S. Kim, *et al.*, "An experimental study on the effect of mesoporous silica addition on ion conductivity of poly(ethylene oxide) electrolytes," *Current Applied Physics*, vol. 8, pp. 729-731, 2008.

[78] Y. X. Jiang, *et al.*, "A novel composite microporous polymer electrolyte prepared with molecule sieves for Li-ion batteries," *Journal of Power Sources* vol. 160, pp. 1320-1328, 2006.

[79] T. Kuila, *et al.*, "Enhancing the ionic conductivity of PEO based plasticized composite polymer electrolyte by LaMnO3 nanofiller," *Materials Science and Engineering B: Solid-State Materials for Advanced Technology*, vol. 137, pp. 217-224, 2007.

[80] J. Xi, *et al.*, "Enhanced electrochemical properties of PEO-based composite polymer electrolyte with shape-selective molecular sieves," *Journal of Power Sources* vol. 156, pp. 581-588, 2006.

[81]   L. J. Alvarez, *et al.*, "Computer simulation of γ-Al₂O₃ microcrystal," *The Journal of Physical Chemistry*, vol. 99, pp. 17872-17876, 1995.

[82]   J.-K. Hyun, *et al.*, "Molecular dynamics simulations and spectroscopic studies of amorphous tetraglyme (CH₃O(CH₂CH₂O)₄CH₃) and tetraglyme: LiCF₃SO₃ structures," *The Journal of Physical Chemistry B*, vol. 105, pp. 3329-3337, 2001.

[83]   O. Borodin and G. D. Smith, "Mechanism of ion transport in amorphous poly(ethylene oxide)/LiTFSI from molecular dynamics simulations," *Macromolecules*, vol. 39, pp. 1620-1629, 2006.

[84]   O. Borodin, *et al.*, "Li⁺ cation environment, transport, and mechanical properties of the LiTFSI doped N-methyl-N-alkylpyrrolidinium⁺TFSI⁻ ionic liquids," *The Journal of Physical Chemistry B*, vol. 110, pp. 16879-16886, 2006.

[85]   O. Borodin, *et al.*, "Li⁺ transport in lithium sulfonylimide−oligo(ethylene oxide) ionic liquids and oligo(ethylene oxide) doped with LiTFSI," *The Journal of Physical Chemistry B*, vol. 110, pp. 24266-24274, 2006.

[86]   F. Müller-Plathe and W. F. Van Gunsteren, "Computer simulation of a polymer electrolyte: Lithium iodide in amorphous poly(ethylene oxide)," *The Journal of Chemical Physics*, vol. 103, pp. 4745-4756, 1995.

[87]   S. Neyertz and D. Brown, "Local structure and mobility of ions in polymer electrolytes: A molecular dynamics simulation study of the amorphous PEOₓNaI system," *The Journal of Chemical Physics*, vol. 104, pp. 3797-3809, 1996.

[88]   O. Borodin, *et al.*, "Force field development and MD simulations of poly(ethylene oxide)/LiBF₄ polymer electrolytes," *The Journal of Physical Chemistry B*, vol. 107, pp. 6824-6837, 2003.

[89]   L. J. A. Siqueira and M. C. C. Ribeiro, "Molecular dynamics simulation of the polymer electrolyte poly(ethylene oxide)/LiClO₄. II. Dynamical properties," *The Journal of Chemical Physics*, vol. 125, pp. 214903-8, 2006.

[90]   M. J. Monteiro, *et al.*, "Transport coefficients, Raman spectroscopy, and computer simulation of lithium salt solutions in an ionic liquid," *The Journal of Physical Chemistry B*, vol. 112, pp. 2102-2109, 2008.

[91]   P. T. Boinske, *et al.*, "Lithium ion transport in a model of amorphous polyethylene oxide," *Journal of Computer-Aided Materials Design*, vol. 3, pp. 385-402, 1996.

[92]   Y. Duan, *et al.*, "Mechanisms of lithium transport in amorphous polyethylene oxide," *The Journal of Chemical Physics*, vol. 122, pp. 054702-8, 2005.

[93]   D. Brandell, *et al.*, "Molecular dynamics simulation of the crystalline short-chain polymer system LiPF$_6$·PEO$_6$(M_w~1000)," *Journal of Materials Chemistry*, vol. 15, pp. 4338-4345, 2005.

[94]   O. Borodin and G. Smith, "Li$^+$ transport mechanism in oligo(ethylene oxide)s compared to carbonates," *Journal of Solution Chemistry*, vol. 36, pp. 803-813, 2007.

[95]   O. Borodin and G. D. Smith, "Molecular dynamics simulations of poly(ethylene oxide)/LiI melts. 1. Structural and conformational properties," *Macromolecules*, vol. 31, pp. 8396-8406, 1998.

[96]   O. Borodin and G. D. Smith, "Molecular eynamics simulations of poly(ethylene oxide)/LiI melts. 2. Dynamic properties," *Macromolecules*, vol. 33, pp. 2273-2283, 2000.

[97]   C. Karlsson, *et al.*, "A SANS study of 3PEG-LiClO$_4$-TiO$_2$ nanocomposite polymer electrolytes," *Macromolecules*, vol. 38, pp. 6666-6671, 2005.

[98]   M. Forsyth, *et al.*, "The effect of nano-particle TiO$_2$ fillers on structure and transport in polymer electrolytes," *Solid State Ionics* vol. 147, pp. 203-211, 2002.

[99]   R. L. Karlinsey, *et al.*, "Dependence of conductivity on the interplay of structure and polymer dynamics in a composite polymer electrolyte," *Journal of Physical Chemistry B* vol. 108, pp. 918-928, 2004.

[100]   O. Borodin, *et al.*, "Molecular dynamics study of nanocomposite polymer electrolyte based on poly(ethylene oxide)/LiBF$_4$," *Modelling and Simulation in Materials Science and Engineering*, vol. 12, pp. S73-S89, 2004.

[101]   H. Kasemagi, *et al.*, "Molecular dynamics simulation of the effect of nanoparticle fillers on ion motion in a polymer host," *Solid State Ionics*, vol. 168, pp. 249-254, 2004.

[102]   D. Brandell, *et al.*, "Molecular dynamics simulation of the crystalline short-chain polymer system LiPF$_6$·PEO$_6$ (M_w~1000)," *Journal of Materials Chemistry*, vol. 15, pp. 4338-4345, 2005.

[103]   D. A. McQuarrie, *Statistical mechanics* 1st ed.: University Science Books, 2000.

[104]   M. P. Allen and D. J. Tildesley, *Computer simulation of liquids*: Oxford University Press, 1987.

[105]   J. S. Rowlinson, *Perfect gas*: Pergamon press Inc., 1963.

[106]   N. Metropolis, *et al.*, "Equation of state calculations by fast computing machines," *The Journal of Chemical Physics*, vol. 21, p. 1087, 1953.

[107] A. Z. Panagiotopoulos, "Direct determination of phase coexistence properties of fluids by Monte Carlo simulation in a new ensemble," *Molecular Physics* vol. 61, pp. 813-826, 1987.

[108] B. Smit, *et al.*, "Computer simulations in the Gibbs ensemble," *Molecular Physics: An International Journal at the Interface Between Chemistry and Physics,* vol. 68, pp. 931-950, 1989.

[109] A. Z. Panagiotopoulos, *et al.*, "Phase equilibria by simulation in the Gibbs ensemble," *Molecular Physics,* vol. 63, pp. 527-545, 1988.

[110] A. Z. Panagiotopoulos, "Direct determination of fluid phase equilibria by simulation in the Gibbs ensemble: A review," *Molecular Simulation,* vol. 9, pp. 1-23, 1992.

[111] R. Auhl, *et al.*, "Equilibration of long chain polymer melts in computer simulations," *The Journal of Chemical Physics,* vol. 119, pp. 12718-12728, 2003.

[112] N. C. Karayiannis, *et al.*, "A novel Monte Carlo scheme for the rapid equilibration of atomistic model polymer systems of precisely defined molecular architecture," *Physical Review Letters,* vol. 88, p. 105503, 2002.

[113] C. D. Wick, *et al.*, "Microscopic Origins for the Favorable Solvation of Carbonate Ether Copolymers in CO_2," *Journal Of The American Chemical Society,* vol. 127, pp. 12338-12342, 2005.

[114] A. Leach, *Molecular modelling: Principles and applications*: Prentice Hall, 2001.

[115] L. Verlet, "Computer "experiments" on classical fluids. I. Thermodynamical properties of Lennard-Jones molecules," *Physical Review,* vol. 159, pp. 98-103, 1967.

[116] D. Frenkel and B. Smit, *Understanding molecular simulation*: Academic Press, 2002.

[117] S. I. Sandler, *An introduction to applied statistical thermodynamics*: Wiley 2010.

[118] C. D. Wick and D. N. Theodorou, "Connectivity-altering Monte Carlo simulations of the end group effects on volumetric properties for poly(ethylene oxide)," *Macromolecules,* vol. 37, pp. 7026-7033, 2004.

[119] J. M. Stubbs, *et al.*, "Transferable potentials for phase equilibria. 6. United-atom description for ethers, glycols, ketones, and aldehydes," *The Journal of Physical Chemistry B,* vol. 108, pp. 17596-17605, 2004.

[120] B. Chen, *et al.*, "Monte Carlo calculations for alcohols and their mixtures with alkanes. Transferable potentials for phase equilibria. 5. United-atom description of primary, secondary, and tertiary alcohols," *The Journal of physical Chemistry B*, vol. 105, pp. 3093-3104, 2001.

[121] J. N. Canongia Lopes, *et al.*, "Modeling ionic liquids using a systematic all-atom force field," *The Journal of Physical Chemistry B*, vol. 108, pp. 2038-2047, 2004.

[122] W. D. Cornell, *et al.*, "A second generation force field for the simulation of proteins, nucleic acids, and organic molecules," *Journal of the American Chemical Society*, vol. 117, pp. 5179-5197, 1995.

[123] O. Borodin and G. D. Smith, "Development of many–body polarizable force fields for Li-battery applications: 2. LiTFSI-doped oligoether, polyether, and carbonate-based electrolytes," *The Journal of Physical Chemistry B*, vol. 110, pp. 6293-6299, 2006.

[124] A. Sutjianto and L. A. Curtiss, "Li^+-diglyme complexes: Barriers to lithium cation migration," *The Journal of Physical Chemistry A*, vol. 102, pp. 968-974, 1998.

[125] S. F. Boys and F. Bernardi, "The calculation of small molecular interactions by the differences of separate total energies. Some procedures with reduced errors," *Molecular Physics*, vol. 19, pp. 553-566, 1970.

[126] R. A. Kendall, *et al.*, "High performance computational chemistry: An overview of NWChem a distributed parallel application," *Computer Physics Communications*, vol. 128, pp. 260-283, 2000.

[127] E. J. Bylaska, *et al.*, "NWChem, A computational chemistry package for parallel computers," 5.0 ed. Richland, Washington 99352-0999, USA: Pacific Northwest National Laboratory, 2006.

[128] O. Borodin and G. D. Smith, "Development of many-body polarizable force fields for Li-battery components: 1. Ether, alkane, and carbonate-based solvents," *The Journal of Physical Chemistry B*, vol. 110, pp. 6279-6292, 2006.

[129] S. Lascaud, "Contribution a l'etude du transport des ions dans les electrolytes polymere.," Ph.D, University of Montreal, Montreal, Quebec, Canada 1996.

[130] M. Marzantowicz, *et al.*, "Conductivity and dielectric properties of polymer electrolytes $PEO:LiN(CF_3SO_2)_2$ near glass transition," *Journal of Non-Crystalline Solids*, vol. 353, pp. 4467-4473, 2007.

[131] M. Marzantowicz, *et al.*, "Crystalline phases, morphology and conductivity of PEO:LiTFSI electrolytes in the eutectic region," *Journal of Power Sources*, vol. 159, pp. 420-430, 2006.

[132] U. Essmann, *et al.*, "A smooth particle mesh Ewald method," *The Journal of Chemical Physics,* vol. 103, pp. 8577-8593, 1995.

[133] T.-M. Chang and L. X. Dang, "Recent advances in molecular simulations of ion solvation at liquid interfaces," *Chemical Reviews,* vol. 106, pp. 1305-1322, 2006.

[134] P. Jungwirth and D. J. Tobias, "Specific ion effects at the air/water interface," *Chemical Reviews,* vol. 106, pp. 1259-1281, 2006.

[135] K. P. Jensen and W. L. Jorgensen, "Halide, ammonium, and alkali metal ion parameters for modeling aqueous solutions," *Journal of Chemical Theory and Computation,* vol. 2, pp. 1499-1509, 2006.

[136] J. I. Siepmann, "A method for the direct calculation of chemical potentials for dense chain systems," *Molecular Physics: An International Journal at the Interface Between Chemistry and Physics,* vol. 70, pp. 1145-1158, 1990.

[137] J. I. Siepmann and D. Frenkel, "Configurational bias Monte Carlo: A new sampling scheme for flexible chains," *Molecular Physics,* vol. 75, p. 59, 1992.

[138] J. J. De Pablo, *et al.*, "Estimation of the chemical potential of chain molecules by simulation," *The Journal of Chemical Physics,* vol. 96, p. 6157, 1992.

[139] D. Frenkel, *et al.*, "Novel scheme to study structural and thermal properties of continuously deformable molecules," *Journal of Physics: Condensed Matter,* vol. 4, p. 3053, 1992.

[140] C. D. Wick and J. I. Siepmann, "Self-adapting fixed-end-point configurational-bias Monte Carlo method for the regrowth of interior segments of chain molecules with strong intramolecular interactions," *Macromolecules,* vol. 33, pp. 7207-7218, 2000.

[141] P. V. K. Pant and D. N. Theodorou, "Variable connectivity method for the atomistic Monte Carlo simulation of polydisperse polymer melts," *Macromolecules,* vol. 28, pp. 7224-7234, 1995.

[142] V. G. Mavrantzas, *et al.*, "End-bridging Monte Carlo: a fast algorithm for atomistic simulation of condensed phases of long polymer chains," *Macromolecules,* vol. 32, pp. 5072-5096, 1999.

[143] H. J. C. Berendsen, *et al.*, "Molecular dynamics with coupling to an external bath," *Journal of Chemical Physics,* vol. 81, pp. 3684-3690, 1984.

[144] S. Sylla, *et al.*, "Electrochemical study of linear and crosslinked POE-based polymer electrolytes," *Electrochimica Acta,* vol. 37, pp. 1699-1701, 1992.

[145] M. Volel, *et al.*, "Influence of sample history on the morphology and transport properties of PEO–Lithium salt complexes," *Macromolecules,* vol. 37, pp. 8373-8380, 2004.

[146] K. Hayamizu, *et al.*, "Pulse-gradient spin-echo ^{1}H, ^{7}Li, and ^{19}F NMR diffusion and ionic conductivity measurements of 14 organic electrolytes containing $LiN(SO_2CF_3)_2$" *The Journal of Physical Chemistry B,* vol. 103, pp. 519-524, 1999.

[147] G. Mao, *et al.*, "Structure of liquid PEO-LiTFSI electrolyte," *Physical Review Letters,* vol. 84, p. 5536, 2000.

[148] Y. Saito, *et al.*, "Ionic conduction mechanisms of polyvinylidenefluoride-hexafluoropropylene type polymer electrolytes with $LiN(CF_3SO_2)_2$," *Journal of The Electrochemical Society,* vol. 147, pp. 1645-1650, 2000.

[149] P. Lightfoot, *et al.*, "Crystal structure of the polymer electrolyte poly(ethylene oxide)$_3$: $LiCF_3SO_3$," *Science, New Series,* vol. 262, pp. 883-885, 1993.

[150] B. Kumar and L. G. Scanlon, "Polymer-ceramic composite electrolytes," *Journal of Power Sources,* vol. 52, pp. 261-268, 1994.

[151] J. McBreen, *et al.*, "New approaches to the design of polymer and liquid electrolytes for lithium batteries," *Journal of Power Sources,* vol. 89, pp. 163-167, 2000.

[152] S. Kim, *et al.*, "An experimental study on the effect of mesoporous silica addition on ion conductivity of poly(ethylene oxide) electrolytes," *Current Applied Physics,* vol. 8, pp. 729-731, 2008.

[153] H. Wu and C. D. Wick, "Computational investigation on the role of plasticizers on ion conductivity in poly(ethylene oxide) LiTFSI electrolytes," *Macromolecules,* vol. 43, pp. 3502-3510, 2010.

[154] M. Baaden, *et al.*, "M^{3+} lanthanide cation solvation by acetonitrile: The role of cation size, counterions, and polarization effects investigated by molecular dynamics and quantum mechanical simulations," *The Journal of Physical Chemistry A,* vol. 104, pp. 7659-7671, 2000.

[155] Stephen L. Mayo, *et al.*, "DREIDING: A generic force field for molecular simulations," *The Journal of Physical Chemistry,* vol. 94, pp. 8897-8909, 1990.

[156] G. Gutiérrez and B. Johansson, "Molecular dynamics study of structural properties of amorphous Al_2O_3," *Physical Review B,* vol. 65, p. 104202, 2002.

[157] B.-K. Choi and Y.-W. Kim, "Conductivity relaxation in the PEO–salt polymer electrolytes," *Electrochimica Acta,* vol. 49, pp. 2307-2313, 2004.

[158] A. Mozalev, *et al.*, "The formation of nanoporous membranes from anodically oxidized aluminium and their application to Li rechargeable batteries," *Electrochimica Acta,* vol. 46, pp. 2825-2834, 2001.

[159] F. Franks and S. F. Mathias, *Biophysics of water: proceedings of a working conference.* New York: Wiley-Interscience, 1982.

[160] S. McLaughlin, "The electrostatic properties of membranes," *Annual Review of Biophysics and Biophysical Chemistry,* vol. 18, pp. 113-136, 1989.

[161] B. H. Honig, *et al.*, "Electrostatic interactions in membranes and proteins," *Annual Review of Biophysics and Biophysical Chemistry,* vol. 15, pp. 163-193, 1986.

[162] C. D. Wick and L. X. Dang, "Diffusion at the liquid–vapor interface of an aqueous ionic solution utilizing a dual simulation technique," *The Journal of Physical Chemistry B,* vol. 109, pp. 15574-15579, 2005.

[163] P. Liu, *et al.*, "On the calculation of diffusion coefficients in confined fluids and interfaces with an application to the liquid–vapor interface of water," *The Journal of Physical Chemistry B,* vol. 108, pp. 6595-6602, 2004.